Chemical Geology 453 (2017) 146–168

Contents lists available at ScienceDirect

Chemical Geology

journal homepage: www.elsevier.com/locate/chemgeo

Neodymium isotopes and concentrations in aragonitic scleractinian cold-water coral skeletons - Modern calibration and evaluation of palaeo-applications

Torben Struve [a,b,*], Tina van de Flierdt [a], Andrea Burke [c,d], Laura F. Robinson [c,e], Samantha J. Hammond [f], Kirsty C. Crocket [a,g], Louisa I. Bradtmiller [c,h], Maureen E. Auro [c], Kais J. Mohamed [i], Nicholas J. White [j]

[a] Department of Earth Science and Engineering, Imperial College London, Exhibition Road, London SW7 2AZ, UK
[b] The Grantham Institute for Climate Change and the Environment, Imperial College London, Exhibition Road, London SW7 2AZ, UK
[c] Woods Hole Oceanographic Institution, 360 Woods Hole Road, Woods Hole, MA 02543, USA
[d] Department of Earth Sciences, Irvine Building, University of St Andrews, St Andrews KY16 9AL, Scotland, UK
[e] School of Earth Sciences, University of Bristol, Wills Memorial Building, Queen's Road, Bristol BS8 1RJ, UK
[f] Department of Environment, Earth and Ecosystems, The Open University, Walton Hall, Milton Keynes MK7 6AA, UK
[g] SAMS, Scottish Marine Institute, Oban, Argyll PA37 1QA, UK
[h] Environmental Studies Department, Macalester College, 1600 Grand Avenue, St. Paul, MN 55105, USA
[i] Departmento Geociencias Marinas y Ordenación del Territorio, Facultad de Ciencias del Mar, Universidad de Vigo, 36310 Vigo, Spain
[j] Bullard Laboratories, Department of Earth Sciences, University of Cambridge, Cambridge CB3 0EZ, UK

ARTICLE INFO

Article history:
Received 23 September 2016
Received in revised form 21 January 2017
Accepted 24 January 2017
Available online 27 January 2017

Keywords:
Neodymium isotopes
Rare earth elements
Cold-water corals
Seawater
Sediments
Drake Passage

ABSTRACT

Cold-water corals (CWCs) are unique archives of mid-depth ocean chemistry and have been used successfully to reconstruct the neodymium (Nd) isotopic composition of seawater from a number of species. High and variable Nd concentrations in fossil corals however pose the question as to how Nd is incorporated into their skeletons.
We here present new results on modern specimens of *Desmophyllum dianthus*, *Balanophyllia malouinensis*, and *Flabellum curvatum*, collected from the Drake Passage, and *Madrepora oculata*, collected from the North Atlantic. All modern individuals were either collected alive or uranium-series dated to be <500 years old for comparison with local surface sediments and seawater profiles. Modern coral Nd isotopic compositions generally agree with ambient seawater values, which in turn are consistent with previously published seawater analyses, supporting small vertical and lateral Nd isotope gradients in modern Drake Passage waters. Two *Balanophyllia malouinensis* specimens collected live however deviate by up to 0.6 epsilon units from ambient seawater. We therefore recommend that this species should be treated with caution for the reconstruction of past seawater Nd isotopic compositions.
Seventy fossil Drake Passage CWCs were furthermore analysed for their Nd concentrations, revealing a large range from 7.3 to 964.5 ng/g. Samples of the species *D. dianthus* and *Caryophyllia* spp. show minor covariation of Nd with ^{232}Th content, utilised to monitor contaminant phases in cleaned coral aragonite. Strong covariations between Nd and Th concentrations are however observed in the species *B. malouinensis* and *G. antarctica*. In order to better constrain the source and nature of Nd in the cleaned aragonitic skeletons, a subset of sixteen corals was investigated for its rare earth element (REE) content, as well as major and trace element geochemistry. Our new data provide supporting evidence that the applied cleaning protocol efficiently removes contaminant lithogenic and ferromanganese oxyhydroxide phases. Mass balance calculations and seawater-like REE patterns rule out lithogenic and ferromanganese oxyhydroxide phases as a major contributor to elevated Nd concentrations in coral aragonite. Based on mass balance considerations, geochemical evidence, and previously published independent work by solid-state nuclear magnetic resonance (NMR) spectroscopy, we suggest authigenic phosphate phases as a significant carrier of skeletal Nd. Such a carrier phase could explain sporadic appearance of high Nd concentrations in corals and would be coupled with seawater-derived Nd isotopic compositions, lending further confidence to the application of Nd isotopes as a water mass proxy in CWCs.

1. Introduction

Aragonitic scleractinian cold-water corals (CWCs) are abundant in regions where availability of other palaeoceanographic archives is

* Corresponding author at: Max Planck Research Group for Marine Isotope Geochemistry, Institute for Chemistry and Biology of the Marine Environment (ICBM), University of Oldenburg, Carl-von-Ossietzky-Str. 9-11, 26129 Oldenburg, Germany.
E-mail address: tstruve@mpi-bremen.de (T. Struve).

http://dx.doi.org/10.1016/j.chemgeo.2017.01.022

limited, such as the mid-depth North Atlantic (e.g., Frank et al., 2004; Robinson et al., 2007) or the mid-depth Southern Ocean (e.g., Burke et al., 2010; Thiagarajan et al., 2013; Margolin et al., 2014). Their skeletons can be dated accurately by uranium-series disequilibrium (e.g., Edwards et al., 1987; Cheng et al., 2000; Robinson et al., 2006), and growth rates from 0.5 to 2 mm/year in *Desmophyllum dianthus* (Risk et al., 2002; Adkins et al., 2004) and up to 26 mm/year in *Lophelia pertusa* (Gass and Roberts, 2006; recently synonymised to *Desmophyllum pertusum*, Addamo et al. 2016) can provide for high resolution geochemical archives (e.g., Adkins et al., 1998; Copard et al., 2012; Montero-Serrano et al., 2013; Wilson et al., 2014; Chen et al., 2015; Hines et al., 2015; Lee et al., 2017).

A powerful proxy to constrain past water mass changes is the neodymium (Nd) isotopic composition of seawater, which has been extracted from various marine archives (e.g., van de Flierdt and Frank, 2010), including CWCs (van de Flierdt et al., 2006a; Robinson and van de Flierdt, 2009; Colin et al., 2010; Copard et al., 2011, 2012; López Correa et al., 2012; Montero-Serrano et al., 2011, 2013; Wilson et al., 2014). While the proxy has been calibrated successfully in both modern colonial (reef - building) and solitary corals (van de Flierdt et al., 2006a; Copard et al., 2010, van de Flierdt et al., 2010), there are a number of questions that still need addressing. Firstly, the global calibration effort by van de Flierdt et al. (2010) was conducted on museum specimens, which were U-Th dated to be between 0 and 377 years old, with two ages however ranging back to the middle and early Holocene. Furthermore, coral Nd isotope results were compared to the most proximal site in the ocean where seawater results were published from the same water mass. In some cases, this was up to 2000 km away from the site of coral collection. A more direct calibration was performed by Copard et al. (2010), who analysed 13 corals collected alive for their Nd isotopic composition. Five of which were directly comparable to nearby seawater measurements. There is still a need to expand the current calibration to include a wider range of coral samples collected alive for comparison with ambient seawater.

Another point that needs revisiting for the application of Nd isotopes in CWCs as a palaeo water mass proxy is the observation of elevated Nd concentrations in thoroughly cleaned fossil coral skeletons (e.g., Crocket et al., 2014). Pioneering calibration studies showed that Nd concentrations in modern CWC specimens of ≤42.7 ng/g (Copard et al., 2010; van de Flierdt et al., 2010) are similar to observations in shallow-water corals (SWC), i.e., ≤55.5 ng/g (Shaw and Wasserburg, 1985; Sholkovitz and Shen, 1995; Akagi et al., 2004; Wyndham et al., 2004). Moreover, Copard et al. (2010) showed a weak dependence of Nd concentrations in modern specimens with water depth, qualitatively in agreement with the behaviour of dissolved Nd in seawater. Fossil specimens however revealed that Nd concentrations in cleaned aragonite can be significantly higher than cited above (up to 612 ng/g in Crocket et al., 2014 and 772 ng/g in Wilson et al., 2014), which has been speculated to result from incomplete removal of contaminant phases (Copard et al., 2010; Crocket et al., 2014). Colin et al. (2010) ruled out contributions from ambient sediments as no systematic relationship between sediment and coral Nd isotopic compositions could be observed downcore. Crocket et al. (2014), on the other hand, performed mass balance calculations to show that contamination from ferromanganese oxyhydroxide phases can account for a maximum of 27% of observed Nd concentration in cleaned aragonite, with no resolvable effect on the Nd isotopic composition. However, as most modern and fossil CWCs show Nd concentrations in excess of what is predicted from inorganic aragonite precipitation experiments (Terakado and Masuda, 1988; ~6–11 ng/g) it is necessary to identify the nature of skeletal Nd.

In this paper we present (i) a new Nd isotope calibration of live CWCs and local seawater from the Drake Passage and a location close to Iceland (Fig. 1), and (ii) a multi-element investigation to identify the dominant Nd carrier phase in CWC skeletons. Taken together our results improve the robustness of the Nd isotope signal extracted from (fossil) aragonitic CWC skeletons.

2. Samples

2.1. Seawater

In order to compare coral data and ambient seawater, three seawater profiles were collected for 10 to 12 depths each during NBP0805 (April to May 2008) on the *R/V Nathaniel B. Palmer* in the Drake Passage using the shipboard CTD system equipped with PVC Niskin bottles (Fig. 1 and Table 1). Ten litre samples were transferred from Niskin bottles into acid cleaned cubitainers using Tygon® tubing. Unfiltered samples were acidified to pH < 2 onboard using high purity HCl. Sampling stations were located in deep waters off Burdwood Bank (north of the Subantarctic Front), off the southern end of the Shackleton Fracture Zone (near the southern boundary of the ACC), and near Sars and Interim seamounts (near the Polar Front; Figs. 1 and 2). All major water masses were sampled: surface mixed layer, Subantarctic Mode Water (SAMW), Antarctic Intermediate Water (AAIW), Upper Circumpolar Deep Water (UCDW), and Lower Circumpolar Deep Water (LCDW) mixing with South Pacific Deep Water (SPDW) and Weddell Sea Deep Water (WSDW) at depth (Fig. 2).

2.2. Sediments

Sediment samples were collected during NBP0805 and NBP1103 (May to June 2011) on the *R/V Nathaniel B. Palmer* from a number of locations across the Drake Passage and at water depths between 333 and 4395 m (Figs. 1 and 2, Table 2). Coring was successful during NBP1103 at Burdwood Bank (Kasten core KC08, 333 m water depth), Interim seamount (Kasten core KC77, 3095 m) and at the WAP margin (Box core BC63, 597 m water depth). During NBP0805 small amounts of sediment samples were collected using a minicorer attached to the CTD to recover sediments from 4221 and 4395 m water depth near Sars and the SFZ, respectively. Additional gravel was collected from two dredges (DR18 and DR35; Table 3) at SFZ (2392 m) and Sars seamount (695 m; Figs. 1 and 2, Table 2). Samples were taken from respective top sections where possible (i.e., not applicable to dredge samples; Table 2). The lithology of the different samples is very heterogeneous reflecting the different depositional environments, but also different sampling methods; for example dredged sediments contain rock fragments. KC08 is characterised as quartz sand, including some darker minerals with an overall slightly green overgrowth. Sediment samples from Sars (DR35 and CTD04 minicore containing mud with pieces of rock) and Interim (KC77, sand) seamounts are dominated by light-brown and grey colours indicating unusually high carbonate contents. Sediments from SFZ (DR18 and CTD03 minicore) are grey to brown and contain mostly mud and rock fragments. BC63 sediments from the WAP contain various grain sizes in a grey-brown mud matrix.

2.3. Cold-water corals

Modern solitary coral specimens of *Desmophyllum dianthus* ($n = 3$), *Balanophyllia malouinensis* ($n = 4$) and *Flabellum curvatum* ($n = 1$; Fig. 3) were collected on Burdwood Bank by dredging and trawling during NBP0805 ($n = 6$ from one Blake Trawl at 816 m water depth) and LMG0605 (May–June 2006) on the *R/V Laurence M. Gould* ($n = 2$; both *B. malouinensis*; one from 120 m water depth and one from 854 m water depth; Figs. 2 and 3; Table 4). It should be noted that 'modern samples' in this case includes specimens collected alive ($n = 3$) and specimens to be <467 years old as confirmed by U-series dating (Table 4; Burke and Robinson, 2012; Burke, 2012; Burke et al., unpubl. data). The shallowest sample from 120 m water depth (*B. malouinensis*) was bathed in subsurface waters of the mixed layer, whereas the samples from 816 m (southern slope of Burdwood Bank) and 854 m water depth (northern slope of Burdwood Bank) were bathed in AAIW (Fig. 2; Table 4). *B. malouinensis* (Fig. 3) is a species that is very abundant

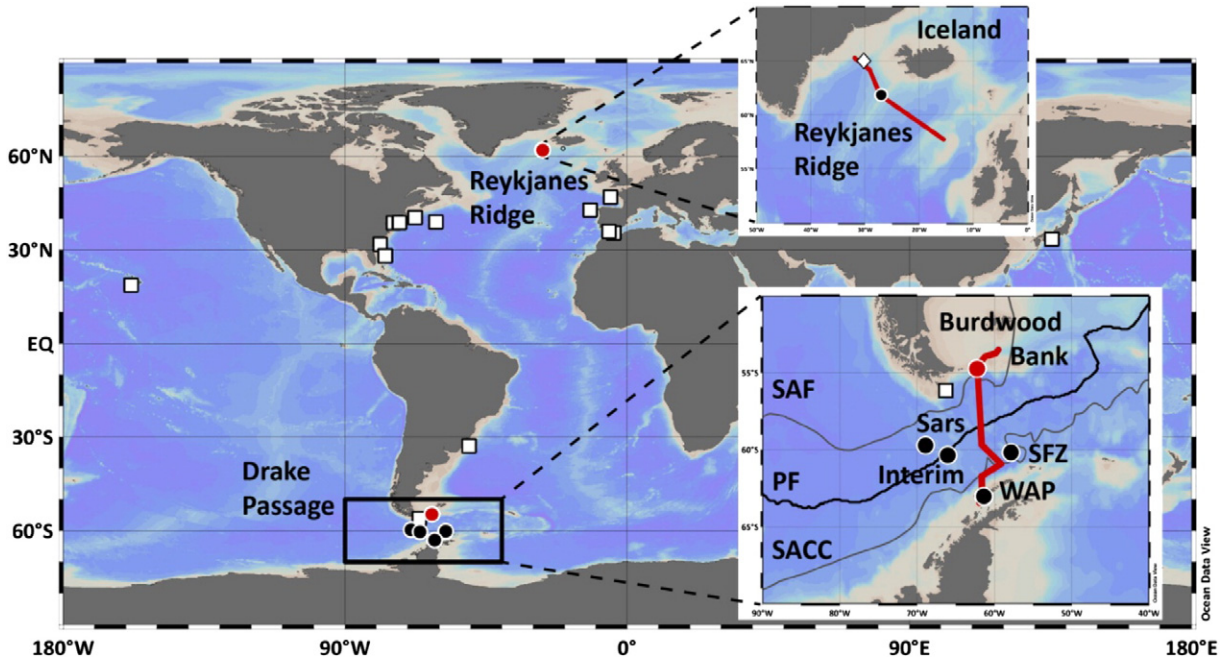

Fig. 1. Global locations of modern CWCs used for calibration of Nd isotopic composition with ambient seawater. White squares indicate sample locations of previous studies (Copard et al., 2010; van de Flierdt et al., 2010). Red dots highlight the locations of Burdwood Bank and Reykjanes Ridge, i.e., calibration places from this study. Red line indicates the trajectory of oxygen (Drake Passage) and potential temperature (Reykjanes Ridge) sections presented in Figs. 2 and 4. White diamond represents location of Northeast Atlantic seawater shown in Fig. 4. Black dots with white outlines denote further (fossil) coral sample locations utilised in this study. Maps generated using ODV software (Schlitzer, 2012). Positions of Southern Ocean fronts from Orsi et al. (1995). SAF: Sub-Antarctic Front; PF: Polar Front; SACC: southern ACC front. SFZ: Shackleton Fracture Zone; WAP: West Antarctic Peninsula.

in the Drake Passage (Margolin et al., 2014), but has not yet been calibrated for Nd isotope work.

One additional modern specimen of the colonial coral *Madrepora oculata* (Figs. 3 and 4) was dredged during cruise CE0806 (April–May 2008) on the *R/V Celtic Explorer* in the North Atlantic at 768 m water depth on the Reykjanes Ridge (61.87°N, 27.01°W; Burke, 2012). This coral was bathed in a mixture of Subpolar Mode Waters (SPMW), Labrador Seawater (LSW), Iceland-Scotland-Overflow Water (ISOW) and North Atlantic Central Waters (NACW; Talley and McCartney, 1982; Lacan and Jeandel, 2004a,b, 2005a; Yashayaev et al., 2007; Fig. 4, Table 4).

In order to investigate the integrity of the Nd isotope signal in fossil CWC aragonite, we selected 70 fossil specimens from the Drake Passage for analysis of their Nd concentrations. The sample set includes the species *Desmophyllum dianthus* ($n = 55$), *Balanophyllia malouinensis* ($n = 8$), *Flabellum curvatum* ($n = 3$), *Gardineria antarctica* ($n = 3$) and *Caryophyllia spp.* ($n = 1$) and was collected by dredging or trawling during cruises NBP0805, NBP1103 and LMG0605 at Burdwood Bank (318 to 1515.5 m), Sars Seamount (695 to 1750 m), Interim Seamount (982.5 to 1195.5 m), and the Shackleton Fracture Zone (SFZ; Figs. 1 and 2, Tables 5 and 6). Uranium-series dates for all fossil samples (Table 6) are taken from previous publications (Burke and Robinson, 2012; Chen et al., 2015), except some U-Th replicate analyses and one yet unpublished coral date (Burke et al.) with ages ranging from 1,100 to 226,000 years before present (kyrs BP). It is noted here that chemistry cuts, from the original piece of coral that was dated, have been analysed for Nd concentrations ('minimum concentrations' – see next section and Struve et al., 2016). Eighteen full chemical replicates of combined U-series and Nd isotope analyses were carried out on sixteen individual corals of the species *D. dianthus*, *Caryophyllia* spp. and *G. Antarctica* (see Table 6). Fourteen of which were re-sampled pieces of the respective coral, and four replicates were generated from split aliquots of a crushed, but still inhomogenous, coral sample (Table 6).

A subset of 16 corals (13 *D. dianthus*, two *B. malouinensis*, and one *G. antarctica*) was re-sampled to investigate major and trace element content and to obtain precise Nd concentration data (Tables 5 and 6).

3. Analytical procedures

3.1. Sample preparation for Nd isotope and concentration analysis

The selected sediment samples were in some cases limited to subgram levels, for example for the top sections of CTD minicorer samples, dredged and box core samples (Table 2); homogenisation may hence be imperfect in such sediments. Sediment samples were exposed to a sequential leaching and digestion procedure following Cook et al. (2013). Briefly, this procedure involved carbonate removal with buffered acetic acid and removal of FeMn oxyhydroxide phases in a mixture of acetic acid and hydroxylamine hydrochloride. No step was performed to remove biogenic opal. Subsamples of ~50 mg sediment (NBP0805 DR35, <300 μm fraction: ~8 mg) were exposed to aqua regia (3:1 mixture of concentrated HCl and HNO_3, respectively) to remove organics, followed by silicate digestion in a mixture of concentrated $HClO_4$, HNO_3, HF and in 0.6:1:2 proportion, after which the samples were converted to chloride form in 1 M HCl. An aliquot containing ~5–6 mg dissolved detritus (~22 mg of sand sample NBP1103 KC08, 0–5 cm) was then spiked with ^{150}Nd spike for subsequent ion exchange chromatography using Biorad® AG50W-X8 resin (200–400 mesh) following Struve et al. (2016). Separation of Nd from other REEs followed the procedure of Cook et al. (2013) and was achieved using Eichrom Ln spec® resin (50–100 μm bead size, modified after Pin and Zalduegui, 1997).

Cold-water coral Nd isotopic data were generated at Imperial College London from ~0.1 to 1.3 g subsamples, either from wash fractions collected during U-Th separation at WHOI or from re-sampled pieces of the same coral specimens used for U-series dating (Tables 4, 5 and 6). Cleaning of re-sampled specimens and those utilised for combined U-Th-Nd extraction followed similar procedures (e.g., Cheng et al., 2000; van de Flierdt et al., 2010; Burke and Robinson, 2012; Crocket et al., 2014). All coral and seawater samples were oxidised with aqua regia, followed by a 1:1 mixture of concentrated HNO_3 and 30% H_2O_2 prior to REE separation in order to remove any residual organics from previous columns and/or initial digestion in 8 M HNO_3. All samples

Table 1
Neodymium isotope results for Drake Passage seawater. All samples were collected during expedition NBP0805 on the R/V Nathaniel B. Palmer. Note that samples were not filtered and that Nd separation was performed on chemistry cuts from Pa-Th ion exchange chromatography. Poor yields for some particular batches led to unusually high internal errors (i.e., low beam sizes; see Auro et al., 2012 and Struve et al., 2016 for details). CTD4 station was located near Sars and Interim seamounts (Fig. 2); B. Bank = Burdwood Bank, SFZ = Shackleton Fracture Zone.

Sample	Lat	Long	Water depth (m)	Location	$^{143}Nd/^{144}Nd$[a]	2SE[b]	ε_{Nd}[c]	2SE	2SD[d]
CTD2_R-2-1	−54.872	−62.140	2190	B. Bank	0.512229	0.000008	−7.97	0.16	0.20
CTD2_R-4-2	−54.872	−62.140	2100	B. Bank	0.512243	0.000016	−7.70	0.32	0.32
CTD2_R-6-3	−54.872	−62.140	1800	B. Bank	0.512245	0.000014	−7.66	0.26	0.26
CTD2_R-12-6	−54.872	−62.140	1200	B. Bank	0.512229	0.000009	−7.97	0.18	0.20
CTD2_R-14-7	−54.872	−62.140	805	B. Bank	0.512220	0.000020	−8.16	0.40	0.40
CTD2_R-16-8	−54.872	−62.140	500	B. Bank	0.512235	0.000015	−7.86	0.30	0.30
CTD2_R-18-9	−54.872	−62.140	300	B. Bank	0.512211	0.000010	−8.33	0.19	0.20
CTD2_R-20-10	−54.872	−62.140	200	B. Bank	0.512213	0.000014	−8.28	0.28	0.28
CTD2_R-21-11	−54.872	−62.140	49	B. Bank	0.512210	0.000020	−8.35	0.39	0.39
CTD2_R-24-12	−54.872	−62.140	0	B. Bank	0.512203	0.000022	−8.48	0.43	0.43
CTD3_R-2-1	−60.617	−56.535	4221	SFZ	0.512249	0.000006	−7.60	0.11	0.20
CTD3_R-4-2	−60.617	−56.535	4105	SFZ	0.512245	0.000004	−7.67	0.08	0.20
CTD3_R-6-3	−60.617	−56.535	3700	SFZ	0.512232	0.000005	−7.92	0.10	0.20
CTD3_R-8-4	−60.617	−56.535	3200	SFZ	0.512218	0.000005	−8.19	0.11	0.20
CTD3_R-10-5	−60.617	−56.535	2500	SFZ	0.512225	0.000005	−8.05	0.10	0.20
CTD3_R-12-6	−60.617	−56.535	1800	SFZ	0.512209	0.000005	−8.36	0.10	0.20
CTD3_R-14-7	−60.617	−56.535	1400	SFZ	0.512204	0.000006	−8.46	0.11	0.20
CTD3_R-16-8	−60.617	−56.535	1000	SFZ	0.512197	0.000006	−8.61	0.12	0.20
CTD3_R-18-9	−60.617	−56.535	410	SFZ	0.512213	0.000006	−8.29	0.12	0.20
CTD3_R-20-10	−60.617	−56.535	249	SFZ	0.512215	0.000006	−8.26	0.12	0.20
CTD3_R-21-11	−60.617	−56.535	100	SFZ	0.512228	0.000006	−7.99	0.11	0.20
CTD3_R-24-12	−60.617	−56.535	8.8	SFZ	0.512233	0.000007	−7.90	0.13	0.20
CTD4_R-2-1	−59.823	−66.003	4395	Sars/Interim	0.512245	0.000007	−7.66	0.14	0.20
CTD4_R-4-2	−59.823	−66.003	4295	Sars/Interim	0.512237	0.000006	−7.81	0.11	0.20
CTD4_R-6-3	−59.823	−66.003	4000	Sars/Interim	0.512249	0.000006	−7.60	0.12	0.20
CTD4_R-8-4	−59.823	−66.003	3500	Sars/Interim	0.512240	0.000007	−7.77	0.14	0.20
CTD4_R-10-5	−59.823	−66.003	2999	Sars/Interim	0.512221	0.000006	−8.13	0.12	0.20
CTD4_R-12-6	−59.823	−66.003	2250	Sars/Interim	0.512214	0.000007	−8.28	0.13	0.20
CTD4_R-14-7	−59.823	−66.003	1499	Sars/Interim	0.512208	0.000013	−8.24	0.25	0.25
CTD4_R-16-8	−59.823	−66.003	1000	Sars/Interim	0.512204	0.000017	−8.46	0.32	0.32
CTD4_R-18-9	−59.823	−66.003	600	Sars/Interim	0.512236	0.000015	−7.84	0.29	0.29
CTD4_R-24-12	−59.823	−66.003	0	Sars/Interim	0.512223	0.000008	−8.09	0.15	0.20

[a] $^{143}Nd/^{144}Nd$ ratios were corrected for the offset of the measured JNdi-1 ratio of 0.512104 ± 0.000010 (n = 115) from the published value of 0.512115 ± 0.000007 (Tanaka et al., 2000).
[b] 2SE is the 2σ standard error of the measurement.
[c] ε_{Nd} was calculated using the present day CHUR value of $^{143}Nd/^{144}Nd$ = 0.512638 (Jacobsen and Wasserburg, 1980).
[d] 2SD refers to the 2σ standard deviation derived from the long term reproducibility of BCR-2 standards over a 26 months period (see text). If the internal 2σ SE was larger than the external one, the internal error is reported.

from U-Th wash fractions processed for Nd isotope analyses were doped with a ^{150}Nd spike after collection to monitor Nd concentrations. This procedure produces a minimum concentration estimate ([Nd_{min}]), which, according to yield tests may underestimate true Nd concentrations in coral aragonite by up to ~12% (Tables 4 and 6; Struve et al., 2016). Coral samples processed for Nd isotope analyses only were spiked after initial digestion in 8 M HNO_3 and yielded accurate Nd concentrations ([Nd]).

Ten litre seawater samples were initially processed by Fe coprecipitation and ion exchange chromatography for Pa-Th separation at WHOI (Auro et al., 2012). Wash fractions from this procedure were subjected to the same ion exchange chromatography as coral samples and outlined in brief below. Samples processed for Nd isotope analyses before April 2014 were dissolved in 1 M HNO_3 and 0.9 M ascorbic acid mixture for REE separation with Eichrom RE spec® resin (100–150 μm). Due to the strong oxidation required after RE spec® chemistry (Crocket et al., 2014; Lambelet et al., 2016) we changed in April 2014 to REE separation using Biorad® AG50W-X8 resin (200–400 mesh). In both cases seawater and coral Nd purification was achieved on a second column using Eichrom Ln spec® resin (20–50 μm) as described by Crocket et al. (2014).

3.2. Neodymium isotope analyses

Neodymium isotope analyses were carried out on a ThermoFinnigan Triton TIMS in the MAGIC laboratories at Imperial College London. Seawater and coral samples, analysed in NdO^+ mode, were loaded in 2 × 0.5 μl 2.5 M HCl on degassed single W filaments between two layers of 0.5 μl TaF_5 activator (Crocket et al., 2014). Sediment Nd isotope analyses, performed in Nd^+ mode, were loaded in 2 × 0.5 μl 2.5 M HCl sandwiched between two layers of 0.5 μl 0.01 M H_3PO_4 on degassed Re filaments in a double filament assembly (e.g., Andreasen and Sharma, 2009). After correcting for isobaric interferences, the instrumental mass bias was corrected for by normalisation to $^{146}Nd/^{144}Nd$ = 0.7219 using an exponential law (Crocket et al., 2014). Barium was monitored manually, but no significant interference was found in any of our samples for the critical mass range of isobaric BaF and BaO. Pure JNdi-1 loads of 5 and 15 ng Nd were analysed in NdO^+ mode (n = 110) and 60 and 100 ng loads in Nd^+ mode (n = 5) over a period of 26 months ($^{143}Nd/^{144}Nd$ = 0.512104 ± 0.000010, n = 115, five per turret) to monitor instrumental offset. To monitor accuracy, 10 and 30 ng Nd loads of USGS BCR-2 reference material were analysed as NdO^+ (n = 32), and one 80 ng load was analysed as Nd^+ yielded. $^{143}Nd/^{144}Nd$ ratios in all samples, as well as the secondary reference material, were corrected for the offset of the within-turret JNdi-1 average from the reference ratio of 0.512115 ± 0.000007 (Tanaka et al., 2000). BCR-2 samples yieled $^{143}Nd/^{144}Nd$ ratios of 0.512637 ± 0.000010 (2SD; n = 33), identical to the value published by Weis et al. (2006). Our in-house coral reference material yielded a similar precision for 10 and 30 ng Nd loads ($^{143}Nd/^{144}Nd$ = 0.512336 ± 0.000009; n = 23). We consider the 2SD uncertainty based on repeat BCR-2 and coral standard runs as most realistic external error for our coral runs, and hence report the 2SD uncertainty from these runs for all our samples. Exceptions were made for sample analyses where the within-run 2SE was higher, which in turn was used on data graphs and in text descriptions.

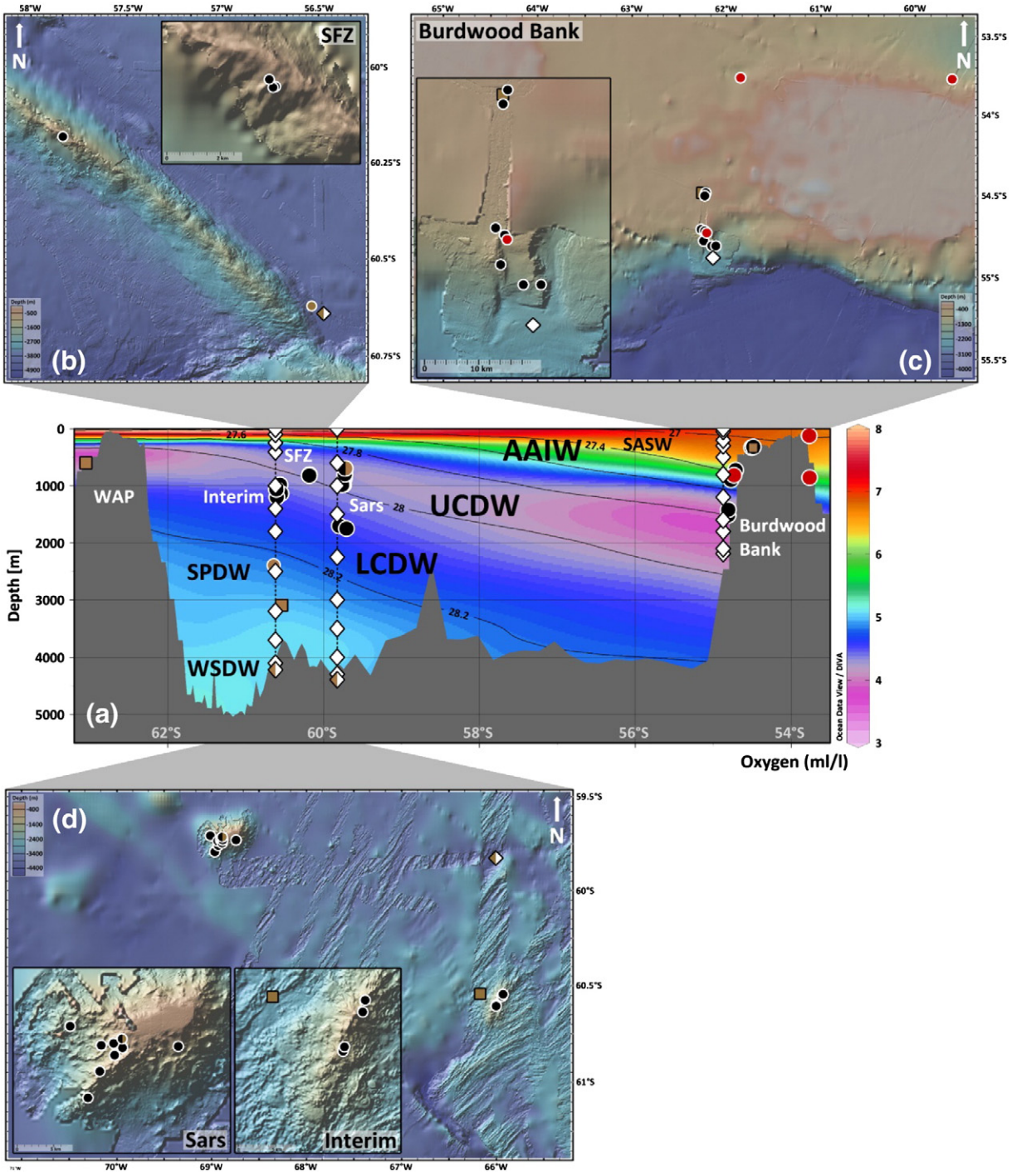

Fig. 2. Seawater, sediment and coral sampling locations in the Drake Passage. (a) Oxygen section across the Drake Passage (red line in Fig. 1; WOA13: Garcia et al., 2013; generated with ODV software; Schlitzer, 2012). White diamonds: seawater profiles; black circles: fossil CWCs; red circles: modern CWCs; brown colour: locations for sediment collection, with symbol type indicating the sampling device, i.e., box or Kasten cores (squares), dredges (dots), minicorer attached to CTD (diamond). Shared symbols indicate multiple samples collected with the same device at respective location. Thin black lines indicate surfaces of neutral density anomaly γ^n (Jackett and McDougall, 1997; in kg/m^3). SASW: Sub-Antarctic Surface Water, AAIW: Antarctic Intermediate Water, UCDW: Upper Circumpolar Deep Water, LCDW: Lower Circumpolar Deep Water, SPDW: South Pacific Deep Water, WSDW: Weddell Sea Deep Water (after Sievers and Nowlin, 1984; Orsi et al., 1999, Sudre et al., 2011) (b) to (d) Detailed bathymetric maps for (b) Shackleton Fracture Zone, (c) Burdwood Bank, and (d) Sars and Interim seamounts. Maps were generated with Geomapapp (http://www.geomapapp.org) using GMRT (Ryan et al., 2009) and high resolution data from NBP0805 and NBP1103 bathymetric surveys (Hoy et al., 2015).

Full procedural blanks of combined U, Th and Nd separation from aragonite matrix ranged from 2 to 27 pg Nd ($n = 20$). Full procedural blanks of combined Pa, Th and Nd separation from seawater matrix were significantly higher at 0.24 and 0.48 ng Nd due to blank problems induced by sample processing (Auro et al., 2012), which were rectified during the later part of our study (e.g., after processing of the seawater samples reported here). Contribution of Nd chemistry to this elevated blank was monitored and found to be below 17 pg Nd ($n = 7$). The Nd isotopic composition of the 0.48 ng full procedural blank was $^{143}Nd/^{144}Nd = 0.512225 \pm 0.000029$ (2SE). Even though blanks contributed up to 25% of the analysed natural sample Nd, blank corrections were found to contribute <0.04 epsilon units and hence no correction was applied. The full procedural Nd blank of the sediment protocol was 13 pg ($n = 1$).

Table 2
Neodymium isotope results for Drake Passage sediments. All samples were collected during two cruises on the *R/V Nathaniel B. Palmer*, NBP0805 and NBP1103, at Burdwood Bank, Sars and Interim seamounts, Shackleton Fracture Zone (SFZ) and the West Antarctic Peninsula (WAP). Samples were analysed as Nd^+ by TIMS at Imperial College London and were spiked with ^{150}Nd after digestion to obtain accurate Nd concentration data by isotope dilution. All analyses were carried out on bulk samples except for sample NBP0805 DR35 of which the <300 μm fraction was analysed. Asterisks indicate potentially contaminated samples, i.e., sample DR35 showed some blue pieces of presumably rubber after digestion and in sample BC63, a soft component appeared during the digestion procedure which could not be classified. These samples are therefore omitted for mixing calculations presented in Section 5.2.1.

Cruise	Event	Device	Lat	Long	Water depth (m)	Sample size (g)	Location	Depth bsf[f]	$^{143}Nd/^{144}Nd$[a]	2SE[b]	ε_{Nd}[c]	2SE	2SD[d]	Nd (μg/g)	2SE[e]
NBP1103	KC08	Kasten corer	−54.486	−62.230	333	6.19	Burdwood Bank	0–5 cm	0.512381	0.000004	−5.02	0.08	0.20	15.82	0.000003
NBP0805	DR35*	Dredge	−59.723	−68.881	695	0.84	Sars seamount	Surface scrapings	0.512658	0.000010	0.38	0.19	0.20	7.49	0.000002
NBP0805	CTD04	Minicorer	−59.823	−66.003	4395	0.07	Near Sars	0–3 cm	0.512488	0.000006	−2.92	0.13	0.20	11.60	0.000012
NBP1103	KC077	Kasten corer	−60.544	−66.177	3095	3.26	Interim	0–5 cm	0.512469	0.000007	−3.29	0.13	0.20	11.89	0.000009
NBP0805	DR18	Dredge	−60.643	−56.472	2392	1.63	SFZ	Surface scrapings	0.512304	0.000006	−6.52	0.11	0.20	21.23	0.000003
NBP0805	CTD03	Minicorer	−60.617	−56.535	4221	0.79	SFZ	coretop	0.512584	0.000007	−1.06	0.14	0.20	15.61	0.000005
NBP1103	BC63*	Boxcorer	−63.054	−61.592	597	0.32	WAP	0–1 cm	0.512764	0.000006	2.46	0.13	0.20	12.81	0.000004

[a] $^{143}Nd/^{144}Nd$ ratios were corrected for the offset of the within-run JNdi-1 average value ($n = 5$) from the published value of 0.512115 ± 0.000007 (Tanaka et al., 2000).
[b] 2SE is the 2σ standard error of the measurement.
[c] ε_{Nd} was calculated using the present day CHUR value of $^{143}Nd/^{144}Nd = 0.512638$ (Jacobsen and Wasserburg, 1980).
[d] 2SD refers to the 2σ standard deviation derived from the long term reproducibility of BCR-2 standards over a 26 months period (see text). If the internal 2σ SE was larger than the external one, the internal error is reported.
[e] 2SE is the propagated 2σ standard error on Nd concentrations determined by isotope dilution.
[f] Below seafloor.

3.3. Major and trace element analyses on modern and fossil corals and sediments

Major and trace element analyses on 16 re-sampled and cleaned fossil and modern coral samples and seven sediment samples were carried out on an Agilent 7500 s ICP-MS, at the Department of Environment, Earth and Ecosystems, Open University. Analyses of coral and sediment samples were carried out in a matrix of 2% nitric acid on unspiked aliquots taken from the fully dissolved samples prior to ion chromatography. Mass 156 ($^{140}Ce^{16}O$) was measured to monitor oxide interferences on the heavy REE. Ratios of 156/140 (CeO/Ce) were low at ~0.4% throughout all analytical sessions. Doubly charged species, measured as 70/140 (Ce^{2+}/Ce^{+}), were below 1.0%.

The sediment samples were analysed during one analytical session, containing USGS reference material BCR-2. Aliquots of dissolved sediment samples were diluted to ~5 ng/g Nd as Nd concentrations were already known from TIMS isotope dilution measurements (see Section 3.1 and Table 2). The deviation from the reference values (Wilson, 1997) was <7% for the elements reported in Table 3.

In order to optimise results of low-abundance trace elements, and in particular lanthanide series elements, aliquots of dissolved coral samples were analysed for their Al, Ca, Ti, Mn and Fe content at ~1000 μg/g Ca level and REE, Th and U at ~2000 μg/g Ca. Coral samples were analysed in four separate runs over two analytical sessions (Table 5). Sample concentrations were calculated using seven in-house multi-element standards doped with Ca to match sample contents. Machine drift was monitored and corrected for with measurement of a monitor block after every five sample analyses consisting of an in-house multi-element standard, a CWC reference material (Crocket et al., 2014) and 2% HNO3 solution to measure instrument background. Full procedural blank levels were negligible for all elements of interest.

Coral reference material 1RSD ($n = 9$) were below 8% for most REE and U, whereas low abundance heavy REE (HREE) reproduced less well (Tm: 31%, Yb: 11% and Lu: 12% 1RSD). The external precision of other elements of interest in our coral reference material were as follows: Th: 15%, Al: 20%, Ca: 7%, Ti: 8%, Mn: 27% and Fe: 13% 1RSD. Limestone reference material JLs-1 was used to monitor reproducibility during 1000 μg/g Ca sessions and is therefore considered relevant only for Al, Ca, Ti, Mn and Fe, but the other values are reported for completeness. The external precision obtained from repeated analyses of JLs-1 ($n = 8$) was better than 7% 1RSD for most elements, except Ti: 16% (omitting one flyer), Sm: 12%, Tb: 15%, Tm: 13% ($n = 4$, below limit of detection during second run), Yb: 8% and Th: 13% 1RSD (Table 5). USGS reference material BCR-2 was measured as an unknown for additional quality control in the beginning and at the end of each analytical session. The external precision of all BCR-2 analyses ($n = 6$, diluted to 5 ng/g Nd) yielded REE results within 5% 1RSD and within 20% 1RSD for most other elements (Al, Ca, Ti, Th and U). Exceptions were Fe (51% 1RSD) and Mn (53% 1RSD).

Four out of the 16 re-sampled corals have furthermore been processed for Nd concentration analyses by TIMS isotope dilution allowing for intercomparison with ICP-MS data (Tables 4 and 6).

4. Results

4.1. Seawater data

The Nd isotopic composition of seawater at all three depth profiles in the Drake Passage falls within a narrow ε_{Nd} range between −7.6 ± 0.2 and −8.6 ± 0.2 (Table 1, Fig. 5; ($\varepsilon_{Nd} = ((^{143}Nd/^{144}Nd_{sample})/(^{143}Nd/^{144}Nd_{CHUR}) - 1) \times 10{,}000$; CHUR: chondritic uniform reservoir, see Jacobsen and Wasserburg, 1980), indicating a relatively homogenous water column signature across the modern Drake Passage. In detail, the two seawater profiles from Sars/Interim seamounts and the SFZ reveal identical ε_{Nd} values within error. Both profiles are characterised by slightly more radiogenic values in surface and bottom waters (average $\varepsilon_{Nd\ (\leq 100\ m)} = -8.0 \pm 0.2$, 2SD, $n = 3$; $\varepsilon_{Nd\ (\geq 3500\ m)} = -7.7 \pm 0.2$, 2SD, $n = 7$) compared to intermediate water depths ($\varepsilon_{Nd\ (1000–2000\ m)} = -8.4 \pm 0.2$, 2SD, $n = 5$). While the seawater profile from the slope off Burdwood Bank reveals the same overall range in Nd isotopic compositions, the most radiogenic values are observed in 1800 to 2190 m water depth (average $\varepsilon_{Nd} = -7.8 \pm 0.3$, 2SD, $n = 3$) and the least radiogenic values are found in the uppermost 300 m of the water column (average $\varepsilon_{Nd} = -8.4 \pm 0.2$, 2SD, $n = 4$). Fig. 5 illustrates that our new seawater Nd isotope results are in excellent agreement with previously published seawater profiles from the Drake Passage, with the exception of a small apparent deviation in deep waters from south of the polar front (Piepgras and Wasserburg, 1982; Stichel et al., 2012).

4.2. Sediment data

Major and trace element data as well as Nd isotopic compositions of detrital sediments collected from across the Drake Passage are reported

Table 3
ICP-MS major and trace metal data of Drake Passage sediment samples generated at the Open University. The sample ID refers to the event ID in Table 2 listing further details. Last three columns denote Ce, Gd and Eu anomalies, calculated using PAAS-normalised values: $Ce/Ce^* = 2 \times Ce_N / (La_N + Pr_N)$, $Gd/Gd^* = 2 \times Gd_N / (Eu_N + Tb_N)$ and $Eu/Eu^* = 2 \times Eu_N / (Sm_N + Gd_N)$. Values used for normalisation (in μg/g): La = 38, Ce = 80, Pr = 8.9, Nd = 32, Sm = 5.6, Eu = 1.1, Gd = 4.7, Tb = 0.77, Dy = 4.4, Ho = 1.0, Er = 2.9, Tm = 0.40, Yb = 2.8, Lu = 0.43 (Taylor and McLennan, 1985). The results of one USGS BCR-2 reference material are reported and compared to the reference values (Wilson, 1997).

Sample ID	Al (%)	Ca (%)	Ti (%)	Mn μg/g	Ba μg/g	La μg/g	Ce μg/g	Pr μg/g	Nd μg/g	Sm μg/g	Eu μg/g	Gd μg/g	Tb μg/g	Dy μg/g	Ho μg/g	Er μg/g	Yb μg/g	Lu μg/g	Th μg/g	U μg/g	Ce/Ce*	Gd/Gd*	Eu/Eu*
KC08	5.8	0.5	0.3	247	556	16.8	38.9	4.4	16.6	3.5	0.8	2.9	0.5	2.5	0.5	1.6	1.6	0.2	5.7	1.9	1.04	0.91	1.22
DR35*	3.5	1.9	0.5	354	1794	7.7	27.3	1.9	7.6	1.6	0.6	1.5	0.2	1.3	0.3	0.7	0.7	0.1	2.8	0.7	1.62	0.75	1.85
CTD04	6.5	1.4	0.4	538	485	12.6	26.4	3.2	12.0	2.6	0.7	2.2	0.4	2.2	0.5	1.4	1.5	0.2	4.0	1.0	0.95	0.83	1.40
KC77	5.3	1.4	0.3	368	1629	15.2	30.9	3.4	12.4	2.5	0.8	2.1	0.4	2.1	0.5	1.4	1.3	0.2	3.9	1.0	0.99	0.77	1.55
DR18	5.4	1.2	0.5	448	364	22.9	52.0	5.9	22.6	4.6	1.0	4.2	0.7	3.8	0.8	2.3	2.3	0.3	8.0	1.4	1.03	0.99	1.06
CTD03	7.0	2.1	0.5	779	363	15.0	32.1	4.1	16.5	4.0	1.1	3.7	0.6	3.8	0.8	2.4	2.3	0.4	4.3	1.4	0.94	0.85	1.37
BC63*	8.1	3.7	0.6	1041	265	11.2	24.1	3.3	14.1	3.6	1.2	3.9	0.7	4.2	0.9	2.7	2.5	0.4	2.8	0.9	0.90	0.85	1.45
BCR-2 ($n = 1$)	7.1	5.2	1.3	1434	707	25.6	53.4	7.0	29.2	6.7	2.1	6.8	1.1	6.0	1.3	3.7	3.6	0.5	5.8	1.6			
Reference value	7.1	5.1	1.4	1520	683	25.0	53.0	6.8	28.0	6.7	2.0	6.8	1.1	–	1.3	–	3.5	0.5	6.2	–			
Difference to reference value (%)	0.8	−1.2	3.5	5.6	3.5	−2.3	−0.8	−2.7	−4.3	−0.7	−6.4	0.5	−1.0	–	0.9	–	−1.8	−2.8	6.6	–			

* Indicate potentially contaminated samples as described in the caption of Table 3.

in Tables 2 and 3. Radiogenic Nd isotope values ranging from $\varepsilon_{Nd} = 2.5 \pm 0.2$ to $\varepsilon_{Nd} = -6.5 \pm 0.2$, as well as positive Eu anomalies ($Eu/Eu^* = 2 \times Eu_N / (Sm_N + Gd_N) = 1.1$ to 1.9; subscript "N" denotes normalisation to Post-Archean Australian Shale (PAAS); Taylor and McLennan, 1985) indicate a significant volcanogenic component in the detrital fraction (see also Noble et al., 2012). Neodymium concentrations are depleted ([Nd] = 11.6 to 21.2 μg/g) in comparison to upper continental crust values ([Nd] = 26 μg/g; Taylor and McLennan, 1985), but within the range of local volcanics from the Antarctic Peninsula and the southern tip of Chile (cf. GEOROC database). The two most positive results in ε_{Nd} stem from two samples (DR35 and BC63; Table 2), which were potentially contaminated and are hence omitted from further discussion and mass balance calculations (see caption of Table 2 for details).

4.3. Cold-water coral data

4.3.1. Modern calibration

The modern North Atlantic specimen of *M. oculata* from 768 m water depth was dated to be no older than 30 years and yielded an ε_{Nd} of -13.1 ± 0.2, which is the least radiogenic Nd isotopic composition obtained during this study and in line with other analyses of CWCs in the North Atlantic. As such it shows excellent agreement with the nearby seawater from west off Iceland (Fig. 6), following the neutral density anomaly $\gamma^n = 27.74$ kg/m^3 ($\varepsilon_{Nd} = -13.2 \pm 0.2$ at 401 m water depth; Station 14, Lacan and Jeandel, 2004a; Figs. 1 and 4). Results for modern specimens of *F. curvatum* (collected alive; $n = 1$), *B. malouinensis* (collected alive and dated to be up to 330 years old; $n = 4$), and *D. dianthus* (up to 467 years old; $n = 3$) span a range of ε_{Nd} values from -7.0 ± 0.2 to -7.6 ± 0.2 (Table 4; Fig. 6). A complete replicate of sample 'Big Beauty' yielded excellent agreement in Nd isotopic composition (Table 4). Overall, four of the specimens investigated show Nd isotopic compositions consistent with ambient seawater. In detail, two *D. dianthus*, one *F. curvatum*, and one *B. malouinensis* yield values within error of seawater at 805 m at Burdwood Bank ($\varepsilon_{Nd} = -8.2 \pm 0.4$; Table 4, Fig. 6). One *D. dianthus* specimen (TB04 Dp-A-02) and two live collected specimens of *B. malouinensis* (Mod. Balano-1 and -2) from the same location however deviate from this value.

One additional *B. malouinensis* (LMG06-05/3-1) collected from the northern flank of Burdwood Bank at 120 m water depth ($\varepsilon_{Nd} = -7.2 \pm 0.2$) is also offset from seawater measured at 200 m water depth on the southern flank of Burdwood Bank ($\varepsilon_{Nd} = -8.3 \pm 0.3$; Tables 1 and 4, Figs. 2 and 6). The latter is the only specimen in this collection showing an offset from seawater $\delta^{234}U = 146.8 \pm 0.1$‰ ($2\sigma_m$, $n = 19$; Andersen et al., 2010), i.e., the initial coral $\delta^{234}U = 111.6 \pm 0.5$‰ indicates open system behaviour (see caption of Table 6 for details) and is hence omitted from Fig. 6 and further discussion.

4.3.2. Trace element systematics

For a total of 8 modern and 70 fossil CWCs from the Drake Passage U and Th concentrations are available from isotope dilution during coral dating (MC-ICP-MS; Burke and Robinson, 2012; Chen et al., 2015; Burke et al., unpubl. data) and [Nd_{min}] from Nd isotope dilution analyses of the wash fractions from the same samples (TIMS; see also Section 3.1). In addition, Table 6 includes replicate U, Th and Nd_{min} concentration results (14 analyses on 13 individual corals) obtained on different pieces/poorly homogenised fragments of the same coral specimen that were individually dated. Another subset of 16 corals was further resampled in order to obtain accurate elemental concentrations (Table 5), four of which were also analysed for accurate TIMS isotope dilution Nd concentrations (Tables 4 and 6).

In modern coral samples, ^{232}Th concentrations are generally low, but vary by approximately one order of magnitude (43 to 377 pg/g; Table 4), whereas Nd concentrations ([Nd_{min}] and [Nd]) are typically higher than [^{232}Th], but less variable with values between 6.7 (5.4 in

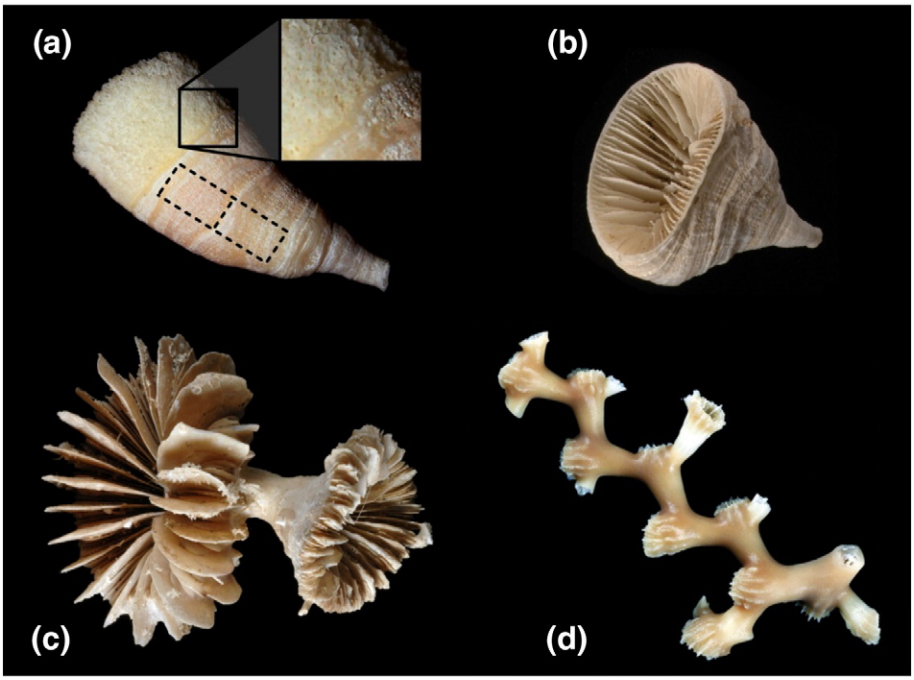

Fig. 3. Pictures of modern CWC specimens from the Drake Passage. (a) *B. malouinensis*, (b) *F. curvatum*, (c) *D. dianthus* collected in the Drake Passage during NBP0805 (photo credit: Dann Blackwood, no scales available) and (d) sub-fossil *M. oculata* (Cairns and Kitahara, 2012). The skeleton of *B. malouinensis* is solid in the lower part and porous at the top (see enlargement of the interface between the two parts of the skeleton). The stippled rectangle in (a) delineates the subsampling areas for upper and lower parts of a fossil *B. malouinensis* skeleton for their trace metal content (Table 5; NBP1103 DH16 Bc-2). Note that the corals shown in this Figure are not the same individuals analysed for this study.

replicate analysis) and 27 ng/g (with the exception of one modern *F. curvatum* with 152.2 ng/g; see Table 4). Among modern coral samples, *D. dianthus* specimen Dp-A-02 and *B. malouinensis* specimen Mod. Balano-1 show the highest ^{232}Th concentrations with 344 pg/g and 377 pg/g, respectively. Modern *B. malouinensis* specimens show a tendency towards elevated ^{232}Th relative to *D. dianthus*, *F. curvatum* and *M. oculata* (Table 4).

The [Nd_{min}] in fossil corals from the Drake Passage ranges from 7.3 ng/g to 964.5 ng/g and ^{232}Th concentrations range from 20 to 3500 pg/g (Table 6, Fig. 7; including the replicate results from isotope dilution). The entire coral [Nd_{min}] and [^{232}Th] dataset (including modern, fossil and replicate coral samples) shows a weak correlation of $R^2 = 0.48$ ($n = 91$, including replicate analyses; Fig. 7). Significantly higher covariations are however observed when isolating the species *B. malouinensis* ($R^2 = 0.96$, $n = 11$) and *G. antarctica* (R^2 near 1, $n = 4$, including replicate analyses; Fig. 7).

The subset of modern and fossil corals analysed for major and trace element concentrations ($n = 16$) yielded the following results: [Al] < 9.2 μg/g, [Ti] < 0.54 μg/g, [Mn] < 0.38 μg/g and [Fe] < 14 μg/g (omitting one result; Table 5). These concentrations are several orders of magnitude lower than in lithogenic and FeMn oxyhydroxide phases (Tables 3 and 5, Fig. 7; Crocket et al., 2014). Despite the large range of Nd concentrations observed in modern and fossil coral specimens, their shale-normalised rare earth element patterns show three distinct features: (i) negative Ce anomalies ($Ce/Ce^* = 2 \times Ce_N / (La_N + Nd_N)$ ranging from 0.03 to 0.09), (ii) enrichment of heavy over light rare earth elements (HREE/LREE = $(Er_N + Yb_N) / (La_N + Nd_N) = 1.1$ to 10), and (iii) slightly positive Gd anomalies ($Gd/Gd^* = 2 \times Gd_N / (Eu_N + Tb_N) = 1$ to 1.3, except for sample NBP0805 DR35 Dc-D002, which shows a negative Gd anomaly (Table 5, Fig. 8). These observations are consistent on intra- and interspecies level, i.e., the REE data set includes *D. dianthus*, *G. antarctica* and *B. malouinensis*.

One fossil specimen of *B. malouinensis* was furthermore subsampled at the upper and lower part of its skeleton (Fig. 3) in order to investigate potential geochemical gradients. The lower part contains about 6 times higher concentrations of lithogenic elements such as Al and Ti, slight enrichment in Nd (38.4 ng/g in the upper part and 52.6 ng/g in the lower part), and similar Fe concentrations (Table 5).

A coral specimen that has not been studied for palaeo work so far is *G. antarctica*. We note that even though REE concentrations seem elevated, the PAAS-normalised pattern (Taylor and McLennan, 1985) resembles the characteristic features of modern seawater (Table 5, Fig. 8).

Four out of the 16 corals resampled for ICP-MS trace element analysis were also analysed for Nd concentrations with isotope dilution and TIMS. The results show good agreement between different analytical methods, i.e., within 6.1% ($n = 3$) and 25.9% for sample NBP0805 TB04 Big Beauty, which shows however very low [Nd] so that the absolute difference between 5.4 and 4.0 ng/g is small (Tables 4, 5 and 6).

The reproducibility of trace metal concentrations in corals can be assessed by comparing U, Th and Nd_{min} concentration results obtained on different pieces of the same coral specimen that were individually dated (see Table 6 and caption). Excluding one outlier, a weak correlation ($R^2 = 0.30$, $n = 12$) is observed for Nd_{min} concentrations obtained from replicate U-Th dating, which only improves marginally when including additional accurate Nd concentration data derived by TIMS isotope dilution ($R^2 = 0.36$, $n = 15$; Fig. 9). In contrast, U concentrations ($R^2 = 0.76$, $n = 12$) and ^{232}Th concentrations ($R^2 = 0.63$, $n = 12$) reproduce better between different parts of the same coral (Table 6, Fig. 9). This observation is corroborated by comparison of Nd_{min} and U concentrations obtained from isotope dilution (Tables 4 and 6) with the corresponding results of the coral subsamples analysed by ICP-MS (Table 5). Excluding two outliers, the [Nd] of two subsamples from the same coral analysed by different methods is only weakly correlated ($R^2 = 0.30$, $n = 14$). In contrast, U concentrations of different subsamples from the same coral show a relatively strong correlation ($R^2 = 0.71$, $n = 15$). The limit of detection of ^{232}Th on the ICP-MS limits a similar comparison with isotope dilution MC-ICP-MS Th data (Table 5).

It is noted that the results presented here were obtained from relatively large samples so that some of the fine scale variability observed previously by Robinson et al. (2006) and Spooner et al. (2016) is averaged out.

Table 4
Neodymium isotopic compositions and U-Th dating of modern coral specimens from the Drake Passage and the North Atlantic. Note that 3 of the samples were collected alive (marked with an asterisk) and that U-Th data are taken from Burke and Robinson (2012), Burke (2012) and Burke et al. (unpubl. data) and reported here for completeness. Neodymium isotope data for this study were generated by processing chemistry cuts from the U-Th ion exchange chromatography through Nd chemistry and analysing them as NdO^+ by TIMS at Imperial College London. As samples were only spiked with ^{150}Nd after U-Th ion exchange chromatography, reported Nd concentrations are minimum estimates (reported in *italic* and as ≥). Yield tests showed that such concentration estimates may be accurate to within ~12% (Struve et al., 2016). Samples Modern-Balano-2 and BigBeauty replicate are newly sampled pieces, in the latter case of the same coral, which were processed for Nd separation only and hence spiked following sample digestion so that reported Nd concentrations are accurate.

Cruise	Event	Sample	Species	Location	Lat	Long	Water depth (m)	Sample mass (g)	Age (years)	2SE[a]	^{238}U (ng/g)	2SE	^{232}Th (pg/g)	2SE	$\delta^{234}U_i$	2SE	$^{143}Nd/^{144}Nd$[b]	2SE	ε_{Nd}[c]	2SE	2SD[d]	Nd (ng/g)	2SE[e]
NBP0805	TB04	Dp-A-02	*D. dianthus*	Burdwood Bank	−54.734	−62.216	816	0.7236	30	71	5445	4	344	7	146.8	0.5	0.512259	0.000007	−7.40	0.13	0.20	*≥11.0*	0.0002
NBP0805	TB04	Dp-A-03	*D. dianthus*	Burdwood Bank	−54.734	−62.216	816	1.3006	66	11	3088	10	43	3	146.8	0.7	0.512247	0.000006	−7.63	0.11	0.20	*≥6.7*	0.0001
NBP0805	TB04	BigBeauty	*D. dianthus*	Burdwood Bank	−54.734	−62.216	816	0.9321	467	20	4539	14	117	2	146.1	0.7	0.512248	0.000008	−7.60	0.15	0.20	*≥7.2*	0.0002
NBP0805	TB04	BigBeauty repl.	*D. dianthus*	Burdwood Bank	−54.734	−62.216	816	0.3039	-	-	-	-	-	-	-	-	0.512252	0.000012	−7.53	0.23	0.23	5.4	0.0008
NBP0805	TB04	Mod.Flabellum*	*F. curvatum*	Burdwood Bank	−54.734	−62.216	816	0.9513	69	13	4893	15	81	3	146.5	0.7	0.512248	0.000004	−7.61	0.07	0.20	*≥152.2*	0.0162
NBP0805	TB04	Mod. Balano-1*	*B. malouinensis*	Burdwood Bank	−54.734	−62.216	816	0.9675	9	78	3737	12	377	2	145.9	0.7	0.512274	0.000005	−7.09	0.10	0.20	*≥14.2*	0.0002
NBP0805	TB04	Mod. Balano-2*	*B. malouinensis*	Burdwood Bank	−54.734	−62.216	816	0.2010	-	-	-	-	-	-	-	-	0.512281	0.000006	−6.97	0.12	0.20	27.0	0.0009
LMG0605	5	20	*B. malouinensis*	Burdwood Bank	−53.763	−59.622	854	0.9665	158	62	4409	3	240	5	146.7	0.6	0.512246	0.000006	−7.64	0.12	0.20	*≥24.5*	0.0002
LMG0605	3	1	*B. malouinensis*	Burdwood Bank	−53.770	−61.860	120	1.0291	330	153	2019	2	263	5	111.6	0.5	0.512271	0.000007	−7.16	0.13	0.20	*≥9.7*	0.0001
CE0806	Dr31A	2	*M. oculata*	Reykjanes Ridge	61.872	−27.008	768	1.0601	-3	25	3775	12	125	1	148.5	0.7	0.511969	0.000008	−13.06	0.20	0.20	*≥14.6*	0.0003

[a] 2SE is the 2σ standard error of the measurement.
[b] $^{143}Nd/^{144}Nd$ ratios were corrected for the offset of the within-run JNdi-1 average value ($n = 5$) from the published value of 0.512115 ± 0.000007 (Tanaka et al., 2000).
[c] ε_{Nd} was calculated using the present day CHUR value of $^{143}Nd/^{144}Nd = 0.512638$ (Jacobsen and Wasserburg, 1980).
[d] 2SD refers to the 2σ standard deviation derived from the long term reproducibility of BCR-2 standards over a 26 months period (see text). If the internal 2σ SE was larger than the external one, the internal error is reported.
[e] 2SE is the propagated 2σ standard error on Nd concentrations determined by isotope dilution.

5. Discussion

5.1. Calibration of modern cold-water corals against ambient seawater

5.1.1. Drake Passage seawater data

Our new seawater data suggest that the vertical water column in the Drake Passage is well mixed (i.e., homogenous) in terms of its Nd isotopic composition, corroborating earlier studies by Stichel et al. (2012) and Piepgras and Wasserburg (1982; Fig. 5). A detailed comparison of our new seawater Nd isotope profiles with those published by Stichel et al. (2012; Fig. 5) reveals however some interesting small deviations in the Nd isotopic composition of waters below 3500 m near the Shackleton Fracture Zone and at Sars/Interim seamounts. Seawater collected in the area during NBP0805 was slightly more radiogenic with average values of $\varepsilon_{Nd\ (\geq 3500\ m)} = -7.7 \pm 0.2$ (2SD, $n = 7$; Fig. 5), compared to waters collected during PS71 (average values of ~−9.0; Stichel et al., 2012). Stichel et al. (2012) ascribed such unradiogenic values to the episodic presence of deep and bottom waters from the nearby Weddell Shelf (Stichel et al., 2012: WSBW/AABW $\varepsilon_{Nd} \approx -9.1$). Such bottom waters are known to fill the deep troughs in the southern Drake Passage and are particularly abundant east of the SFZ as indicated by an oxygen maximum at depth (Sievers and Nowlin, 1984; Sudre et al., 2011; Fig. 2). Hydrographic properties below 3500 m at SFZ during NBP0805 ($\theta \approx -0.24$ °C, salinity of 34.66 psu, $[O_2] \approx 4.9$ ml/l; Dalziel, 2015) are however not consistent with pure Weddell Sea Bottom Water (e.g., Sudre et al., 2011, and references therein), and rather indicate admixture of deep and bottom water masses sourced from the South Pacific (Sievers and Nowlin, 1984; Sudre et al., 2011). A stronger influence of South Pacific deep and bottom waters west of the PS71 transect in the open Drake Passage is supported by our new Nd isotope data, which are consistent with seawater Nd isotope data from the South Pacific (Carter et al., 2012; Rickli et al., 2014; Basak et al., 2015) and hydrographic observations (cf. Sudre et al., 2011). This supports the idea of spatial and/or temporal variability in Southern Ocean seawater Nd isotopic compositions at depth levels influenced by underlying bottom waters (van de Flierdt et al., 2006b).

In contrast, overlying CDW shows no indication of inter-basin heterogeneity. Its average ε_{Nd} value of -8.2 ± 0.5 (2SD, $n = 15$) for our new seawater profiles is identical to results for CDW from previous work in the Drake Passage (Piepgras and Wasserburg, 1982; Stichel et al., 2012; Fig. 5) and in the Pacific sector of the Southern Ocean (Carter et al., 2012; Rickli et al., 2014; Basak et al., 2015). However, as noted by Rickli et al. (2014), the full range of circum-Antarctic LCDW salinity and temperature range is not yet characterised for its Nd isotopic composition. While some of our new results may indicate the influx of Pacific-derived water masses at depths of ~2000 m at Burdwood Bank ($\varepsilon_{Nd} = -7.7 \pm 0.3$ at 1800 and 2100 m water depth, respectively; Table 1, Figs. 2 and 5; see also Well et al., 2003; Brearley et al., 2014), such detailed interpretations have to remain tentative, as seawater samples were not filtered.

Lastly, our small dataset does not show evidence for any significant radiogenic input from and/or boundary exchange (Lacan and Jeandel, 2005a,b) with proximal continental margin sediments (i.e., Burdwood Bank) or topographic features in the Drake Passage such as ridges and seamounts (Fig. 2). This conclusion is reached on the Nd isotopic composition alone, as no precise Nd concentration data are available for our seawater samples.

5.1.2. Calibrating modern cold-water corals with seawater neodymium isotope data

A vital question for using CWCs as a palaeoceanographic archive is whether different species of CWCs are reliable recorders of ambient seawater. Towards this end our new data represent a valuable addition to existing trace metal work in CWC (see Robinson et al., 2014 for a review). With the exception of one specimen, all of the nine analyses on modern CWC samples yielded Nd concentrations ([Nd] = 5.4 to

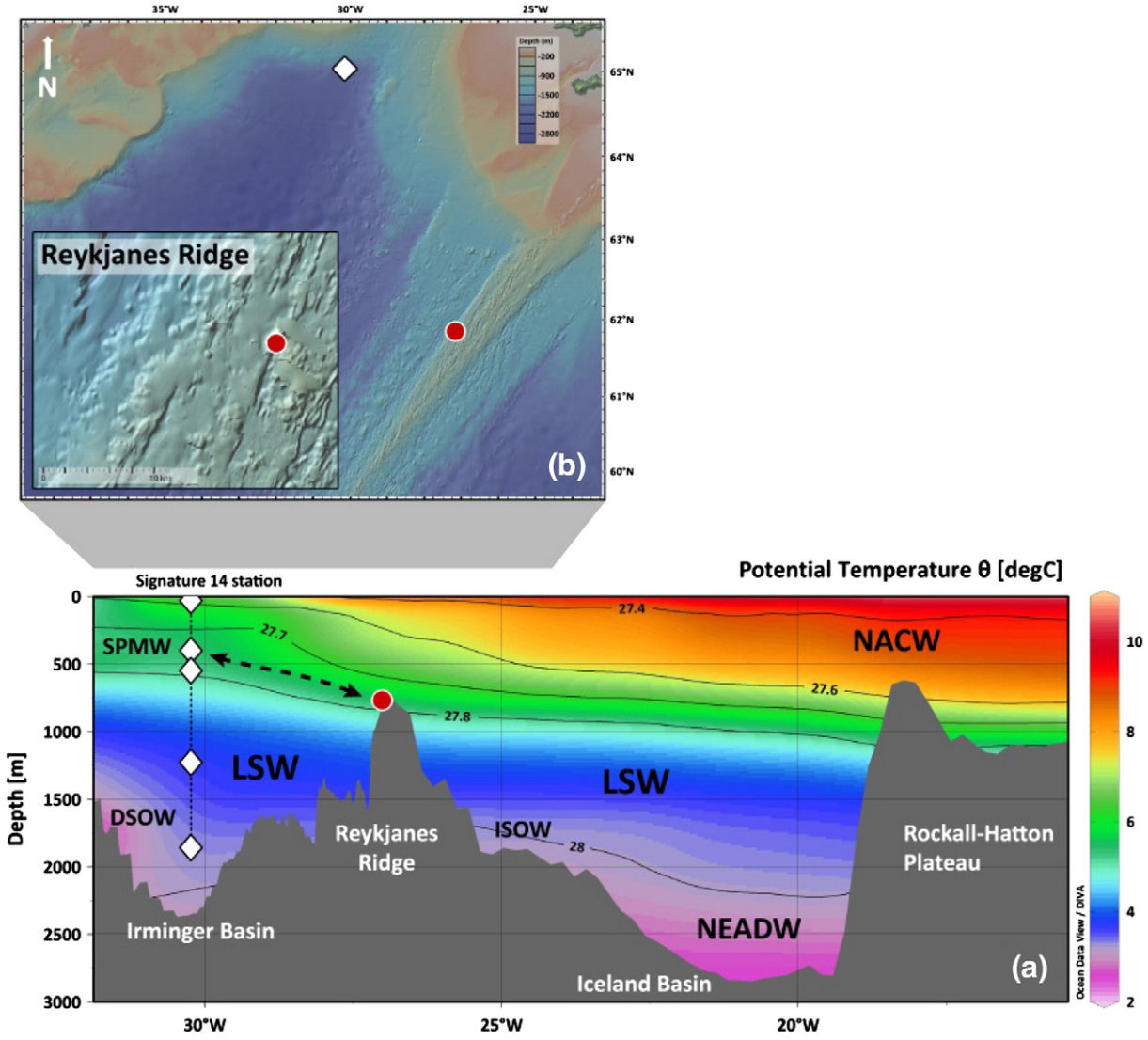

Fig. 4. Sample location for coral collection on the Reykjanes Ridge in the North Atlantic (red circle). White diamonds indicate seawater measurements at signature station 14 from Lacan and Jeandel (2004a, 2005a). (a) Section of potential temperature across the Northeast Atlantic (red line in Fig. 1; WOA13: Locarnini et al., 2013; generated using ODV software; Schlitzer, 2012). Thin black lines indicate surfaces of neutral density anomaly γ^n (Jackett and McDougall, 1997; in kg/m^3). Black stippled line with arrowheads approximates mixing along γ^n = 27.74 kg/m^3. NACW: North Atlantic Central Water, SPMW: Subpolar Mode Water, LSW: Labrador Sea Water, NEADW: Northeast Atlantic Deep Water, ISOW: Iceland Scotland Overflow Water, DSOW: Denmark Strait Overflow Water. Water masses after Talley and McCartney (1982), Lacan and Jeandel (2004a, 2005a) and Yashayaev et al. (2007). (b) Reykjanes Ridge bathymetry map generated with GeoMapApp (http://www.geomapapp.org) using GMRT (Ryan et al., 2009).

27.0 ng/g, [Nd_{min}] = 6.7 to 24.5 ng/g; Table 4) that fall within the lower part of the concentration range previously reported for modern aragonitic scleractinia ([Nd] ≤ 42.7 ng/g, van de Flierdt et al., 2010; Copard et al., 2010; ≤ 92.7 ng/g in a 508 year old specimen, Copard et al., 2011). This includes four *B. malouinensis*, a species previously not investigated for Nd. In terms of their Nd isotopic composition, five out of the eight considered modern specimens from the Drake Passage and the North Atlantic (excluding one *B. malouinensis* due to its very low $\delta^{234}U_i$) overlap with ambient seawater values within analytical uncertainty (Fig. 6, inset).

In detail, *M. oculata* from the North Atlantic shows excellent agreement with ambient seawater, but results from the Drake Passage indicate that some CWC specimens may not incorporate a pure bottom water signature (Fig. 6, inset). The live collected *F. curvatum* specimen overlaps with seawater from 805 m water depth (AAIW depth range, Fig. 2) and is thus considered to reliably record seawater Nd isotopic composition even though the [Nd_{min}] = 152.2 ng/g of this sample falls outside the Nd concentration range reported previously in modern CWCs (this study; van de Flierdt et al., 2010; Copard et al., 2010, 2011, 2012). Of the three *D. dianthus* analysed, two individuals reproduce modern seawater signatures. Sample TB04 Dp-A-2 (a 30-year old *D. dianthus* specimen from 816 m water depth) however reveals a small offset of 0.15 epsilon units from ambient seawater (inset of Fig. 6), which seems at odds with the successful calibration of this species by van de Flierdt et al. (2010). This offset can be accounted for when considering the ^{232}Th concentration relative to the Nd concentration of this sample (344 pg/g and 11.0 ng/g, respectively). Most marine carbonates, including CWC skeletons, are thought to derive their Th content from seawater, adsorbed either during formation or thereafter, but can contain additional and significant contaminant Th from detrital sediment (e.g., Cheng et al., 2000; Robinson et al., 2004).

We use ^{232}Th concentrations obtained for coral specimen TB04 Dp-A-2 to calculate hypothetical maximum contamination of the seawater-derived signal from inclusion of detrital phases in the coral aragonite (see also Section 5.2.1 for details). To simulate the most extreme contamination case, we assume that all detected ^{232}Th in the coral aragonite is sourced from such detrital inclusions. The Nd concentration and

Table 5
Major and trace element data for 17 subsamples from 16 Drake Passage CWCs. All results were obtained at the Open University by ICP-MS on digests of re-sampled pieces of original corals, including two modern (*italic*) and 14 fossil specimens. One fossil specimen was re-sampled twice at the top and lower section, denoted "up" (upper part) and "lp" (lower part), respectively. Ce, Gd, and Eu anomalies and HREE/LREE ratios were calculated from PAAS-normalised results (see caption Table 3). Results were obtained during two analytical sessions comprising two runs each. During the first session Al, Ca, Ti, Mn and Fe were analysed at 1000 μg/g Ca level. The rare earth elements, thorium and uranium were analysed at 2000 μg/g Ca level during the second analytical session. LOD denotes the limit of detection calculated for each particular run during the respective analytical session. Our in-house coral reference material (Crocket et al., 2014) and GSJ reference material JLs-1 (Imai et al., 1996; Igarashi et al., 2003) were matched with sample Ca levels and analysed during the analytical sessions to assess reproducibility. JLs-1 was only analysed at 1000 μg/g Ca level so that only Al, Ca, Ti, Mn and Fe results are considered relevant (see also analytical section for details). Note that one outlier in the Ti results was excluded for RSD calculations on JLs-1. In addition, USGS reference material BCR-2 (Wilson, 1997) results are reported. Coral species: All sample names starting with a 'D' and 'Big Beauty' are *D. dianthus*, 'B' stands for *B. malouinensis*, and 'G' abbreviates *G. antarctica*. Affixes 'a' and 'c' for sample NBP0805 DR35 Dc-A-2 refer to two individual corals, one grown on top of the other.

Cruise	Event	Sample	Sample mass (g)	Al (μg/g)[a]	Ca (%)	Ti (μg/g)[a]	Mn (μg/g)[a]	Fe (μg/g)[a]	La (ng/g)[b]	Ce (ng/g)[b]	Pr (ng/g)[b]	Nd (ng/g)[b]	Sm (ng/g)[b]	Eu (ng/g)[b]
Batch 1														
NBP0805	*TB04*	*Big Beauty*	*0.3039*	*<LOD*	*36.74*	*0.03*	*<LOD*	*7.2*	*8.3*	*<LOD*	*0.9*	*4.0*	*<LOD*	*1.0*
NBP0805	*TB04*	*modern Balano-2*	*0.2010*	*7.5*	*37.21*	*0.54*	*<LOD*	*9.5*	*43.8*	*<LOD*	*5.6*	*26.0*	*4.4*	*1.6*
NBP0805	DR35	Dc-A-2c	0.0260	0.3	37.12	0.06	<LOD	7.8	78.1	<LOD	8.2	36.7	7.4	2.9
NBP1103	DH16	Bc-2 (up)	0.0334	1.5	37.74	0.08	<LOD	10.9	59.6	<LOD	8.0	38.4	8.5	2.7
NBP1103	DH74	Gc-2	0.0484	<LOD	38.14	0.30	<LOD	9.1	581.0	27.5	76.2	350.3	68.4	18.5
NBP0805	DR35	Dc-D4	0.1065	<LOD	37.75	0.08	<LOD	9.4	93.1	<LOD	10.1	46.9	8.5	2.7
NBP0805	DR35	Dc-E1	0.7371	<LOD	36.75	0.13	<LOD	7.9	78.7	<LOD	9.4	39.9	7.1	2.2
NBP0805	DR38	Dc-A1	0.3478	0.3	37.00	0.09	<LOD	10.3	99.4	<LOD	13.1	55.4	8.3	3.2
Batch 1 LOD				0.3	–	0.04	58.0	–	1.6	3.8	0.5	2.0	1.8	0.5
Batch 2														
NBP0805	DR35	Dc-D002	0.5604	0.5	35.31	0.06	<LOD	1.4	90.9	6.0	9.7	43.4	7.7	3.2
NBP0805	DR36	Dc-A2	0.1311	<LOD	36.74	0.08	<LOD	4.5	131.4	<LOD	15.3	75.5	12.0	4.8
NBP1103	DH16	Bc-2 (lp)	0.0418	9.2	36.93	0.51	<LOD	11.0	94.5	4.7	11.2	52.6	12.3	3.5
NBP0805	DR35	Dc-A-2a	0.2039	<LOD	37.00	0.02	<LOD	5.9	48.2	<LOD	5.1	23.9	4.4	1.8
NBP0805	DR23	Dc-A2	0.1522	<LOD	36.37	0.18	0.38	13.8	554.5	26.2	75.0	342.8	61.1	14.8
NBP0805	DR23	Dc-A6	0.0447	0.6	39.43	0.29	<LOD	10.8	86.0	<LOD	10.0	58.0	18.9	9.5
NBP1103	DH117	Dc-29	0.7930	<LOD	37.36	0.11	<LOD	9.4	105.9	<LOD	12.8	60.9	11.3	3.3
NBP0805	DR35	Dc-A1	0.0667	<LOD	37.04	<LOD	<LOD	9.2	10.6	<LOD	0.9	4.7	<LOD	0.9
NBP0805	TB04	Dn-A10	0.1082	8.1	38.39	0.39	<LOD	33.1	128.1	18.6	15.8	77.4	17.0	6.8
Batch 2 LOD				0.2	–	0.06	0.09	–	1.46	3.46	0.43	1.80	1.63	0.49
Reproducibility of reference materials														
Coral standard		average		14.0	20.7	0.6	0.7	24.2	447.3	88.2	56.9	248.5	32.9	6.6
(n = 9)		1SD		2.7	1.4	0.05	0.2	3.2	16.9	3.2	1.6	6.8	2.0	0.5
		1RSD (%)		20	7	8	27	13	4	4	3	3	6	8
		Reference value		15.7	23.1	0.2	0.9	11.9	489.0	100.0	63.0	264.0	–	–
		Difference (%)		−11	−10	224	−30	104	−9	−12	−10	−6	–	–
JLs-1		average		67.8	33.7	1.5	13.0	85.7	82.1	137.5	18.9	76.1	17.3	23.6
(n = 8)		1SD		2.3	0.9	1.2	0.9	3.3	2.7	5.9	0.7	2.6	2.1	1.3
		1RSD %		3	3	16	7	4	3	4	4	3	12	5
		Reference value		109.6	39.3	12.0	16.2	117.5	95.5	201.5	21.5	81.3	17.8	4.2
		Difference (%)		−38	−14	−88	−20	−27	−14	−32	−12	−6	−3	460
BCR-2*		average		5.7	4.9	1.2	0.2	11.0	25.0	53.6	6.8	28.7	6.6	2.0
(n = 6)		1SD		1.1	0.5	0.1	0.1	5.6	0.9	1.9	0.3	0.8	0.2	0.1
		1RSD (%)		20	10	12	53	51	3	4	4	3	3	5
		Reference value		7.1	5.1	1.4	0.15	9.7	25.0	53.0	6.8	28.0	6.7	2.0
		Difference (%)		−20	−4	−9	25	14	0	1	0	2	−2	1

(a) BCR-2 in %
(b) BCR-2 values in μg/g
[#] Including the BCR-2 results obtained from the sediment analyses (listed separately in Table 3) during which Fe and Tm data were not analysed.

isotopic composition of this contamination can in turn be approximated using the Nd results from Kasten corer sediments retrieved on Burdwood Bank (Table 2). Our simple calculation yields a maximal sediment-derived contamination of −0.41 epsilon, which would be sufficient to account for the isotopic offset of −0.15 epsilon units outside analytical uncertainty from seawater observed for this specimen. Similarly, the fact that corals populate on the radiogenic side of analytical uncertainty of seawater Nd isotopic composition (Fig. 6) indicates that contamination may be present in other specimens, but only to an insignificant extent. Contamination from skeletal FeMn oxyhydroxide coatings is considered unlikely to significantly affect the Nd isotopic composition of modern corals as such coatings should carry a modern seawater signal. We hence corroborate the result of previous studies that the aragonitic skeletons of both, *F. curvatum* and *D. dianthus*, are reliable recorders of seawater Nd isotopic compositions once potential contamination is rendered minor and/or accounted for through mass balance correction.

The species *B. malouinensis* has not yet been calibrated for its Nd isotopic composition. Two specimens collected alive and one additional specimen dated to be recently dead (158 years BP; Table 4) show a range of ~0.7 epsilon units in their Nd isotopic composition. The least radiogenic value of -7.6 ± 0.2 was obtained for specimen LMG0605/5-20 from 854 m water depth and overlaps with modern seawater ($\varepsilon_{Nd} = -8.2 \pm 0.4$; Fig. 6, inset). The remaining *B. malouinensis* from 816 m water depth (Mod. Balano-1 and Mod. Balano-2, Table 4) however show ε_{Nd} values of -7.1 ± 0.2 and -7.0 ± 0.2 respectively, significantly more radiogenic than ambient seawater ($\varepsilon_{Nd} = -8.2 \pm 0.4$).

We consider two possible mechanisms to explain these deviations of skeletal Nd isotopic compositions from seawater values. Firstly, the offset may be related to contaminant sources of radiogenic Nd. Indeed, core-top sediment collected from Burdwood Bank is characterised by a Nd isotopic composition of -5.0 ± 0.2 (Table 2), and one of the two corals shows elevated [^{232}Th] (377 pg/g) relative to [Nd_{min}] (14.2 ng/g), as discussed above for a *D. dianthus* specimen. Furthermore,

Gd (ng/g)[b]	Tb (ng/g)[b]	Dy (ng/g)[b]	Ho (ng/g)[b]	Er (ng/g)[b]	Tm (ng/g)[b]	Yb (ng/g)[b]	Lu (ng/g)[b]	Th (ng/g)[b]	U (ng/g)[b]	Ce/Ce*	Gd/Gd*	Eu/Eu*	HREE/LREE
Batch 1													
<LOD	*<LOD*	*2.1*	*0.1*	*1.8*	*<LOD*	*1.8*	*<LOD*	*1.1*	*4056*	–	–	–	*3.75*
7.5	*1.0*	*7.5*	*1.2*	*4.9*	*<LOD*	*4.7*	*0.4*	*<LOD*	*4142*	–	*1.16*	*1.20*	*1.72*
14.9	1.7	14.0	3.1	12.0	<LOD	11.2	1.1	<LOD	3329	–	1.31	1.16	2.55
13.3	1.3	13.5	2.4	9.1	<LOD	8.2	0.7	<LOD	4311	–	1.34	1.14	2.19
93.7	11.4	74.7	15.9	44.0	4.5	34.4	4.5	1.5	4496	0.03	1.26	1.05	1.05
12.3	1.6	11.6	2.3	9.1	0.2	7.8	0.7	<LOD	3467	–	1.16	1.18	1.50
10.6	1.1	10.7	2.1	9.4	<LOD	8.2	0.9	4.1	4304	–	1.31	1.13	1.86
13.0	1.6	12.5	2.5	9.6	<LOD	9.0	0.9	<LOD	5181	–	1.11	1.36	1.50
2.2	0.4	1.8	0.6	0.3	0.6	0.8	0.5	0.4	3.2				
Batch 2													
8.8	1.5	10.6	2.4	8.6	2.3	6.1	0.7	<LOD	3217	0.04	0.78	1.77	1.37
19.8	2.4	18.1	4.1	13.9	1.6	9.4	1.1	<LOD	3180	–	1.12	1.39	1.40
18.6	2.6	23.5	4.2	13.9	1.4	10.1	0.7	1.4	3795	0.03	1.20	1.04	2.03
6.8	0.8	7.0	1.4	7.2	0.8	5.8	0.4	<LOD	3350	–	1.09	1.49	2.25
67.3	8.6	52.6	10.7	30.6	3.2	22.6	2.4	<LOD	4358	0.03	1.17	1.07	0.74
63.4	9.6	75.4	19.1	63.2	8.2	52.4	7.9	<LOD	3619	–	1.28	1.03	9.94
13.4	2.0	15.4	2.7	12.3	1.3	10.3	1.1	<LOD	3541	–	1.02	1.22	1.69
<LOD	<LOD	<LOD	<LOD	2.5	<LOD	2.7	<LOD	<LOD	3865	–	–	–	4.29
40.1	5.9	43.4	10.2	35.4	4.5	28.6	3.7	0.7	2681	0.09	1.24	1.07	3.87
2.02	0.33	1.65	0.52	0.66	0.52	0.71	0.46	0.40	2.92				
Reproducibility of reference materials													
31.0	3.2	19.4	3.8	11.7	1.1	8.9	1.1	3.9	2014				
2.1	0.2	1.3	0.3	0.8	0.3	1.0	0.1	0.6	88				
7	6	7	8	7	31	11	12	15	4				
–	–	–	–	–	–	–	–	4.8	2.4				
–	–	–	–	–	–	–	–	−19	−14				
20.2	2.6	17.4	2.9	11.3	1.7	10.9	1.5	15.0	1356				
1.2	0.4	0.8	0.2	0.8	0.2	0.9	0.2	1.9	24.3				
6	15	5	6	7	13	8	16	13	2				
22.6	3.0	19.3	4.1	13.9	1.9	14.1	2.6	16.0	1830				
−11	−14	−10	−29	−19	−12	−23	−41	−7	−26				
7.0	1.0	6.4	1.3	3.8	0.5	3.5	0.5	6.6	1.2				
0.2	0.04	0.3	0.04	0.2	0.01	0.1	0.04	0.5	0.2				
3	4	5	3	4	3	2	7	8	16				
6.8	1.1	–	1.3	–	0.5	3.5	0.5	6.2	1.7				
3	−2	–	−2	–	−5	1	−1	6	−28				

[^{232}Th] and [Nd_{min}] in fossil *B. malouinensis* specimens show a strong positive correlation ($R^2 = 0.96$, $n = 11$, Fig. 7), which may relate to the porous structure of the skeletons, and in particular the top section (Fig. 3), making the cleaning of *B. malouinensis* skeletons challenging. In contrast to *D. dianthus*, which is known to preferentially live exposed on hard substrates (e.g., Cairns et al., 2005), *B. malouinensis* is either weakly attached to coarse substrate or sits in seafloor sediment as indicated by a cornutiform base (Squires, 1961; Cairns, 1982). This living environment paired with a skeletal structure susceptible to detrital contamination is reflected by geochemical results obtained from sub-sampling fossil *B. malouinensis* specimen NBP1103 DH16 Bc-2 at the upper and lower part of its solid skeleton (Fig. 3). Concentrations of Al and Ti are 6 to 7 times higher in the lower part (Table 5), indicating potential sedimentary contamination and/or interaction with porewaters.

In order to test for sedimentary contamination we use mass balance calculations, assuming a ^{232}Th-free modern coral skeleton and sediments as a sole source of contaminant Th (see Section 5.2.1 for details). Maximum detrital contamination can only account for a Nd isotope shift of up to −0.29 epsilon units, which is insufficient to achieve overlap with modern seawater at the coral collection site. This supports speculations that porewaters may play an additional role. Marine porewaters imply ^{232}Th concentrations higher than overlying bottom waters and are presumably in sorption equilibrium with the solid phase (Cochran et al., 1986). Therefore, the Th isotopic composition of porewaters is likely dominated by the signature of accessible adsorbed FeMn phases and thus similar to ambient seawater values (cf. Chabaux et al., 1997; Robinson et al., 2008). In contrast, batch experiments revealed strong alteration of the dissolved REE budget from detrital release (cf. Pearce et al., 2013; Abbott et al., 2015). Hence, porewater Th may carry seawater-like Th isotope signatures, but paired with a significant detrital REE component. The impact of such porewaters may be amplified by the porous and complex nature of the skeletal structure of *B. malouinensis* (Squires, 1961; Case et al., 2010; cf. also Brahmi et al., 2010 for *B. regia*; Fig. 3), a hypothesis which could however only be tested with

direct porewater samples from the coral sampling locations. Nevertheless, the less porous skeletons of *F. curvatum* (Fig. 3), which can also thrive in the sediment (Squires, 1961), do not show a Nd isotopic offset from ambient seawater values (van de Flierdt et al., 2010; this study). This indicates that the skeletal structure seems to be an important factor for trace metal uptake.

Alternatively, the Nd isotope offset may be related to coral growth rate and thus the length of the time integrated in a particular subsample (i.e., the slower the coral growth rate, the longer the time interval recorded in subsamples of a given size). Adkins et al. (2004) presented vertical extension rates of ~0.5 to 2 mm/year for *D. dianthus*, which hence integrates Nd isotope signals over a time interval of up to ~100 to 200 years. In contrast, growth rates for the species *M. oculata* are up to about one order of magnitude higher (e.g., Orejas et al., 2008; Sabatier et al., 2012) than in *D. dianthus*, significantly reducing the time-integrated signal in a given subsample. Growth rates for *B. malouinensis* are unconstrained, but mature *Balanophyllia regia* specimens of the same genus extend by ~1 mm/year (Brahmi et al., 2010), similar to growth rates observed for mature Flabellum specimens *F. alabastrum* and *F. impensum* (Hamel et al., 2010; Henry and Torres, 2013). Therefore, if *B. malouinensis* specimens live for a long time, and grow very slowly, they would integrate temporal water mass variability. In the case of the Drake Passage, the specimens in question were recovered from a water depth bathed by AAIW, a water mass which is known for its temporal variability and the involvement of water bodies with a more radiogenic signature (Jeandel, 1993; Carter et al., 2012; Stichel et al., 2012 supplement). Such a scenario could resolve the apparent contradiction of seawater-like REE patterns displayed by *B. malouinensis* (e.g., enrichment in HREE, negative Ce anomaly, and positive Gd anomaly, Tables 4 and 5) and non-seawater-like Nd isotopic compositions.

Regardless, both hypotheses have to remain speculative and hence *B. malouinensis*, and potentially other species with porous skeletons living (partly) within the sediments, should be excluded from palaeoclimatic applications for Nd isotopes (and possibly other trace metals) until further constraints become available.

5.2. Neodymium carrier phases in coral aragonite

The Nd concentrations reported here for modern CWC skeletons fall mostly within the range of previously published results (e.g., Copard et al., 2010, 2011, 2012; van de Flierdt et al., 2010). But what does this concentration range mean and how representative is it? Rare earth elements in seawater are predominantly present as carbonate complexes (e.g., Cantrell and Byrne, 1987). Early work assumed that this would favour direct incorporation into the aragonitic lattice of corals (e.g., Shaw and Wasserburg, 1985; Sholkovitz and Shen, 1995). Distribution constants (K_D; cf. IUPAC, 2014) of 1.2 to 2.1 for Nd seemed to support this idea, but inorganic precipitation experiments have expanded this range (Nd $K_D \approx 4$ to 4.5, Terakado and Masuda, 1988). Subsequent studies showed Nd concentrations with maximum values of up to 55.5 ng/g in aragonitic SWC skeletons, but their K_D values were usually <5 (Sholkovitz and Shen, 1995; Akagi et al., 2004; Wyndham et al., 2004). In contrast, Copard et al. (2011, 2012) reported relatively high Nd concentrations of up to 110.1 ng/g in CWCs implying K_D values of up to ~50 which are comparable to the results of one alive collected *F. curvatum* specimen ($[Nd_{min}] = 152.2$ ng/g; Table 4; $K_D = 99$). One caveat in evaluating this concentration range is that even including our new results, the number of concentration analyses performed on modern and recently dead CWC specimens is relatively small (107 analyses on 55 individual solitary and colonial corals, not including samples from sediment cores; Colin et al., 2010; Copard et al., 2010, 2011, 2012; van de Flierdt et al., 2010; Montero-Serrano et al., 2013; this study). We can, however, extend the database by including fossil CWCs (126 analyses on 88 individual solitary and colonial corals, not including samples from sediment cores; Colin et al., 2010; Copard et al., 2010, 2011, 2012; van de Flierdt et al., 2010; Crocket et al., 2014; Wilson et al., 2014; this study).

Minimum and accurate Nd concentrations in 99 subsamples of 70 fully-cleaned fossil coral specimens analysed for this study alone range from 4.7 to 964.5 ng/g (note different analytical methods; see Tables 5 and 6). Moreover, different parts of individual coral specimens, resampled, cleaned and reanalysed, show Nd concentrations deviating by up to ~615 ng/g in *G. antarctica* and ~280 ng/g in *D. dianthus* (Tables 5 and 6; Fig. 9). A similar observation (e.g., intraskeletal Nd variability from a few ng/g up to ~50 ng/g in *D. dianthus*) was also noted by Copard et al. (2010) (based on pers. comm. by P. Montagna) and is evident from Nd concentrations in different subsamples of the same coral (e.g., Copard et al., 2012). Interestingly, variable Nd concentrations seem not to translate to variable Nd isotopic compositions (i.e., excellent reproducibility between different pieces of the same coral specimen; not shown), indicating the carrier phase responsible for elevated Nd concentrations may be authigenic in origin. In the following, we will first evaluate the role of lithogenic and FeMn phases for the coral skeleton Nd budget, then focus on an assessment of organic matter and authigenic precipitates (i.e., phosphates) as potential Nd carrier.

5.2.1. Tracing contaminant Nd carrier phases in coral skeletons

Contaminant Nd carrier phases in coral skeletons are here defined as ferromanganese oxyhydroxide coatings and terrigenous grains (i.e. detritus). Both phases have the potential to compromise the integrity of the seawater-derived primary signal, acquired during coral skeleton growth. Compared to aragonitic coral skeletons, Nd concentrations in FeMn coatings are 3–4 orders of magnitude higher (e.g., Bau et al., 1996; Crocket et al., 2014; Figs. 7 and 8), and Nd concentrations in detrital phases are ~2–3 orders of magnitude higher (e.g., Taylor and McLennan, 1985; Table 3). Even though it is not clear whether the seawater-derived, authigenic Nd is directly incorporated into the aragonitic skeleton, detrital phases could lead to contamination of ambient seawater, either antemortem or post-mortem. The latter could also apply to secondary precipitates such as FeMn oxyhydroxides. Fig. 7 illustrates that elements such as Th, Al, Fe, and Ti, which all have been used as indicators of contamination (e.g., Cheng et al., 2000; Frank et al., 2004; Case et al., 2010; van de Flierdt et al., 2010; Copard et al., 2010; Crocket et al., 2014), are significantly less abundant in CWC samples than in local sediments and FeMn coatings. Moreover, neither Al, nor Fe or Ti concentrations in cleaned coral aragonite show any significant covariation with Nd concentrations (Fig. 7; Table 5; $R^2 < 0.08$). Crocket et al. (2014) furthermore suggested the Ce anomaly (Ce/Ce^*) as a sensitive tracer for contamination in cleaned coral aragonite (Fig. 8) as a pronounced negative Ce anomaly is characteristic of seawater due to oxidation of Ce^{3+} to the insoluble Ce^{4+} under oxic conditions (e.g., Elderfield and Greaves, 1982; De Baar et al., 1985; Sholkovitz et al., 1994). As Ce concentrations are low in cleaned coral skeletons (e.g., often below the limit of detection; Table 5), Ce/Ce^* could only be calculated for five coral samples (Fig. 7). These results are consistent with Ce anomalies observed in modern global deep waters, including results from nearby Drake Passage seawater (Hathorne et al., 2015, and references therein). In summary, contaminant source tracers such as Al, Fe, Ti, Th and Ce/Ce^* do not indicate significant contribution from contaminant sources to clean coral skeletons.

We can further test this statement by reverting to the extensive ^{232}Th concentration dataset (Burke and Robinson, 2012; Chen et al., 2015; Burke et al., unpubl. data; Table 6), as ^{232}Th seems to be the only contaminant source tracer that shows some covariation with $[Nd_{min}]$ in corals (Fig. 7; $R^2 = 0.48$, $n = 91$, including replicates and modern corals). Following the reasoning in Section 5.1.2, we adopted the approach from Crocket et al. (2014) to calculate ^{232}Th-based maximum contribution of $[Nd]_{contamination}$ to $[Nd_{min}]$, assuming that coral aragonite contains no ^{232}Th so that all ^{232}Th can be attributed to contaminant sources. In order to calculate a ^{232}Th-based maximum proportion of contaminant Nd in a physically and chemically cleaned coral subsample we use the

Table 6
Neodymium concentration results for fossil CWC specimens from the Drake Passage. All 70 fossil specimens were collected during cruises NBP0805, NPB1103 and LMG06-05 and processed through U-Th ion exchange chromatography for dating purposes, including 14 full U-Th dating replicates. Neodymium concentrations generated from U-Th column chemistry cuts yielded minimum Nd concentrations (Nd_{min}; see caption of Table 4). Three additional fossil corals were re-sampled for TIMS isotope dilution analysis yielding accurate Nd concentrations, but no U-Th data (denoted with #). Replicate samples are highlighted in bold. Samples are grouped by species and second order by location. All U and Th results are taken from Burke and Robinson (2012), Chen et al. (2015) or unpublished data from Burke et al. and reported here for completeness. Closed $U_{aragonite}$ system behaviour can be monitored with initial $\delta^{234}U_{coral}$ ($\delta^{234}U_i$) reflecting the value of ambient seawater, i.e., 147 ± 7‰ for corals younger than 17 kyrs BP and 141.7 ± 7.8‰ for corals older than 17 kyrs BP (Reimer et al., 2009).

Cruise	Event	Sample	Species	Location	Lat	Long	Depth (m)	Sample mass (g)	^{238}U (ng/g)	2SE[a]	^{232}Th (pg/g)	2SE	$\delta^{234}U_i$	2SE	Nd (ng/g)	2SE[b]
NBP0805	TB04	Dn-*A*-12	*D. dianthus*	B. Bank	— 54.734	— 62.216	816	0.5804	3126	10	3237.4	12.8	149.6	1.0	≥*98.1*	0.0011
NBP0805	TB04	Dn-*A*-11	*D. dianthus*	B. Bank	— 54.734	— 62.216	816	0.6110	3646	12	784.5	2.9	149.2	0.8	≥*87.9*	0.0013
NBP0805	TB04	Dn-*A*-13	*D. dianthus*	B. Bank	— 54.734	— 62.216	816	0.6351	3921	13	175.4	3.2	149.4	0.7	≥*9.3*	0.0002
NBP0805	TB04	Dn-D-6	*D. dianthus*	B. Bank	— 54.734	— 62.216	816	0.6664	3744	12	185.9	1.1	153.3	0.7	≥*24.3*	0.0002
NBP0805	TB04	Dn-B-4	*D. dianthus*	B. Bank	— 54.734	— 62.216	816	0.6357	3920	13	629.2	3.3	153.1	0.8	≥*45.6*	0.0006
NBP0805	TB04	Dn-E-3	*D. dianthus*	B. Bank	— 54.734	— 62.216	816	0.7319	4727	16	181.3	5.5	148.1	0.8	≥*10.1*	0.0001
NBP0805	TB04	Dn-*A*-10a	*D. dianthus*	B. Bank	-— 54.734	— 62.216	816	0.3377	3125	10	1217.6	6.1	155.5	0.8	≥*50.1*	0.0004
NBP0805	**TB04**	**Dn-*A*-10b***	***D. dianthus***	**B. Bank**	**— 54.734**	**— 62.216**	**816**	**0.6317**	**3112**	**10**	**736.8**	**2.5**	**157.7**	**0.8**	**≥*39.2***	**0.0002**
NBP0805	DR40	Dc-*A*-1	*D. dianthus*	Sars	— 59.732	— 68.933	1323	0.7697	3680	11	251.8	1.8	145.1	0.7	≥*57.2*	0.0008
NBP0805	DR35	Dc-A-1a	*D. dianthus*	Sars	— 59.723	— 68.881	695	1.1426	3723	14	120.3	1.5	146.0	0.8	≥*10.9*	0.0001
NBP0805	**DR35**	**Dc-A-1b**	***D. dianthus***	**Sars**	**— 59.723**	**— 68.881**	**695**	**1.1126**	**4163**	**27**	**159.1**	**1.3**	**145.8**	**1.3**	**≥*23.8***	**0.0002**
NBP0805	DR34	Dc-A-2	*D. dianthus*	Sars	— 59.733	— 68.743	869	1.0447	4089	22	232.6	1.3	149.4	1.1	≥*90.2*	0.0060
NBP0805	DR34	Dc-A-1	*D. dianthus*	Sars	— 59.733	— 68.881	869	0.6169	3875	12	313.4	1.3	150.9	0.7	≥*75.9*	0.0013
NBP0805	DR35	Dc-C-2	*D. dianthus*	Sars	— 59.723	— 68.881	695	1.1910	4191	19	183.6	1.1	153.3	1.0	≥*15.3*	0.0002
NBP0805	DR35	Dc-D-4	*D. dianthus*	Sars	— 59.723	— 68.881	695	0.5816	4062	13	224.0	1.2	150.5	0.7	≥*36.0*	0.0004
NBP0805	DR35	Dc-D-5	*D. dianthus*	Sars	— 59.723	— 68.881	695	0.6451	3918	14	323.1	4.4	150.6	0.8	≥ *47.0*	0.0005
NBP0805	DR36	Dc-A-1	*D. dianthus*	Sars	— 59.707	— 69.008	1750	0.7086	4057	13	206.7	2.3	150.5	0.7	≥ *38.9*	0.0004
NBP0805	DR35	Dc-D-1	*D. dianthus*	Sars	— 59.723	— 68.881	695	0.6187	4506	16	157.4	8.4	149.3	0.8	≥*27.3*	0.0003
NBP0805	DR35	Dc-D-3	*D. dianthus*	Sars	— 59.723	— 68.881	695	0.5463	4312	14	226.2	7.9	148.6	0.7	≥*39.7*	0.0003
NBP0805	DR35	Dc-B-1a	*D. dianthus*	Sars	— 59.723	— 68.881	695	0.9327	5852	21	334.8	2.4	147.8	0.8	≥*22.5*	0.0002
NBP0805	**DR35**	**Dc-B-1b**	***D. dianthus***	**Sars**	**— 59.723**	**— 68.881**	**695**	**0.5730**	**4713**	**16**	**393.5**	**4.7**	**147.3**	**0.7**	**≥*44.6***	**0.0004**
NBP0805	DR35	Dc-A-2c+	*D. dianthus*	Sars	— 59.723	— 68.881	695	1.0374	3887	14	551.3	1.8	149.9	0.8	≥*91.4*	0.0023
NBP0805	DR35	Dc-C-1a	*D. dianthus*	Sars	— 59.723	— 68.881	695	0.6913	4259	14	302.3	1.9	148.3	0.7	≥*28.1*	0.0002
NBP0805	**DR35**	**Dc-C-1b***	***D. dianthus***	**Sars**	**— 59.723**	**— 68.881**	**695**	**0.8933**	**4427**	**16**	**303.5**	**1.4**	**147.2**	**0.8**	**≥*23.1***	**0.0002**
NBP0805	DR39	Dc-A-1	*D. dianthus*	Sars	— 59.729	— 68.901	798	0.8002	6545	27	1040.0	3.6	147.3	0.9	≥*53.1*	0.0005
NBP0805	DR38	Dc-A-1	*D. dianthus*	Sars	— 59.743	— 68.898	978	0.6612	6026	22	916.0	3.4	146.2	0.8	≥ *51.1*	0.0007
NBP0805	DR35	Dc-E-1a	*D. dianthus*	Sars	— 59.723	— 68.881	695	0.5033	4234	14	788.1	3.2	150.4	0.8	≥ *76.1*	0.0008
NBP0805	**DR35**	**Dc-E-1b***	***D. dianthus***	**Sars**	**— 59.723**	**— 68.881**	**695**	**0.6319**	**4949**	**17**	**649.7**	**2.5**	**147.3**	**0.8**	**≥*38.2***	**0.0004**
NBP0805	**DR35**	**Dc-E-1c#**	***D. dianthus***	**Sars**	**— 59.723**	**— 68.881**	**695**	**0.7371**	—	—	—	—	—	—	***42.4***	**0.0003**
NBP0805	DR36	Dc-A-2a	*D. dianthus*	Sars	— 59.707	— 69.008	1750	0.7749	3828	13	349.9	1.6	150.0	0.8	≥*73.5*	0.0015
NBP0805	**DR36**	**Dc-A-2b#**	***D. dianthus***	**Sars**	**— 59.707**	**— 69.008**	**1750**	**0.1311**	—	—	—	—	—	—	***80.4***	**0.0010**
NBP1103	DH120	Dc-25	*D. dianthus*	Sars	— 59.797	— 68.965	1701	0.3520	3756	7	508.5	2.1	148.3	0.4	≥*96.1*	0.0004
NBP0805	DR36	Dc-A-3	*D. dianthus*	Sars	— 59.707	— 69.008	1750	0.6101	4116	13	472.3	2.1	148.4	0.7	≥*138.6*	0.0042
NBP1103	DH120	Dn-1a	*D. dianthus*	Sars	— 59.797	— 68.965	1701	0.3040	5022	9	709.7	3.0	147.6	0.4	≥*145.5*	0.0006

(continued on next page)

Table 6 (*continued*)

Cruise	Event	Sample	Species	Location	Lat	Long	Depth (m)	Sample mass (g)	^{238}U (ng/g)	2SE[a]	^{232}Th (pg/g)	2SE	$\delta^{234}U_i$	2SE	Nd (ng/g)	2SE[b]
NBP1103	**DH120**	**Dn-1b**	***D. dianthus***	**Sars**	**— 59.797**	**— 68.965**	**1701**	**0.2765**	**5071**	**9**	**753.1**	**3.1**	**148.0**	**0.4**	**≥*147.6***	**0.0006**
NBP1103	DH120	Dc-33	*D. dianthus*	Sars	— 59.797	— 68.965	1701	0.1843	4260	12	429.9	2.1	146.9	4.7	≥*133.2*	0.0006
NBP1103	DH120	Dc-21a	*D. dianthus*	Sars	— 59.797	— 68.965	1701	0.2007	4046	7	455.9	1.9	149.1	0.4	≥*129.9*	0.0007
NBP1103	**DH120**	**Dc-21b**	***D. dianthus***	**Sars**	**— 59.797**	**— 68.965**	**1701**	**0.2246**	**4054**	**7**	**494.5**	**2.1**	**148.7**	**0.4**	**≥*129.8***	**0.0006**
NBP1103	DH117	Dn-7	*D. dianthus*	Sars	— 59.764	— 68.936	981	0.2727	3659	10	362.9	1.7	152.0	4.7	≥*114.8*	0.0004
NBP1103	DH117	Dc-20	*D. dianthus*	Sars	— 59.764	— 68.936	981	0.3099	3473	6	1041.4	4.3	152.0	0.5	≥*263.1*	0.0019
NBP1103	DH117	Dc-29a	*D. dianthus*	Sars	— 59.764	— 68.936	981	0.4441	4196	10	305.1	1.4	151.2	4.3	≥*29.5*	0.0003
NBP1103	**DH117**	**Dc-29b**[#]	***D. dianthus***	**Sars**	**— 59.764**	**— 68.936**	**981**	**0.7930**	**—**	**—**	**—**	**—**	**—**	**—**	***61.8***	**0.0003**
NBP0805	DR35	Dc-A-2a[+]	*D. dianthus*	Sars	— 59.723	— 68.881	695	0.4737	4761	16	376.7	6.8	148.1	0.7	≥*53.7*	0.0005
NBP0805	DR35	Dc-D-2	*D. dianthus*	Sars	— 59.723	— 68.881	695	0.1780	3743	13	159.9	6.7	227.6	3.2	≥*38.1*	0.0012
NBP1103	DH120	Dc-32	*D. dianthus*	Sars	— 59.797	— 68.965	1701	0.3711	3976	7	537.9	2.3	147.7	0.4	≥*164.5*	0.0011
NBP1103	DH117	Dc-36	*D. dianthus*	Sars	— 59.764	— 68.936	981	0.1498	3673	11	259.7	1.4	153.9	4.6	≥*43.7*	0.0007
NBP1103	DH117	Dc-9a	*D. dianthus*	Sars	— 59.764	— 68.936	981	0.1900	4729	13	1773.4	8.2	146.5	4.5	≥*118.5*	0.0007
NBP1103	**DH117**	**Dc-9b**	***D. dianthus***	**Sars**	**— 59.764**	**— 68.936**	**981**	**0.2493**	**4695**	**8**	**2027.5**	**8.4**	**147.4**	**0.5**	**≥*274.8***	**0.0012**
NBP1103	DH74	Dc-3	*D. dianthus*	Interim	— 60.606	— 66.004	1064	0.1546	3820	12	949.7	4.5	151.4	4.8	≥*124.5*	0.0014
NBP1103	DH75	Dc(f)-37	*D. dianthus*	Interim	— 60.601	— 66.002	1195.5	0.1120	4354	8	668.4	2.9	148.3	0.4	≥*244.8*	0.0009
NBP1103	DH74	Dc-4	*D. dianthus*	Interim	— 60.606	— 66.004	1064	0.2133	4158	7	1878.7	7.8	155.5	0.6	≥*304.7*	0.0010
NBP0805	DR27	Dc-A-1	*D. dianthus*	Interim	— 60.547	— 65.949	1134	0.2010	5919	19	1452.8	11.4	144.3	0.8	≥*261.3*	0.0007
NBP0805	DR27	Dc-A-2	*D. dianthus*	Interim	— 60.547	— 65.949	1134	0.1737	5338	17	1900.4	6.4	148.1	1.0	≥*317.7*	0.0006
NBP0805	DR23	Dc-A-6	*D. dianthus*	SFZ	— 60.182	— 57.834	819	0.2241	4060	13	349.6	4.0	153.2	0.7	≥*48.3*	0.0007
NBP0805	DR23	Dc-A-5	*D. dianthus*	SFZ	— 60.182	— 57.834	819	0.2959	3388	11	625.2	2.5	146.4	0.7	≥*81.8*	0.0013
NBP0805	DR23	Dc-A-7	*D. dianthus*	SFZ	— 60.182	— 57.834	819	0.3702	4183	14	602.9	2.4	149.1	0.7	≥*128.3*	0.0055
NBP1103	DH40	Dc-3a	*D. dianthus*	SFZ	— 60.179	— 57.837	806	0.1034	3671	12	1346.2	6.6	150.0	4.6	≥*151.2*	0.0015
NBP1103	**DH40**	**Dc-3b**	***D. dianthus***	**SFZ**	**— 60.179**	**— 57.837**	**806**	**0.0850**	**3654**	**7**	**2871.3**	**11.9**	**148.8**	**0.6**	**≥*430.9***	**0.0016**
NBP1103	DH43	Dc-6	*D. dianthus*	SFZ	— 60.182	— 57.833	823	0.1130	3337	11	1361.9	6.7	143.5	4.8	≥*145.6*	0.0016
NBP0805	DR23	Dc-A-4	*D. dianthus*	SFZ	— 60.182	— 57.834	819	0.0798	3527	12	1499.3	9.2	143.9	0.8	≥*279.0*	0.0021
NBP1103	DH43	Dc-1	*D. dianthus*	SFZ	— 60.182	— 57.833	823	0.1409	5679	11	162.2	1.8	144.6	0.4	≥*65.3*	0.0009
NBP1103	DH40	Dc-5	*D. dianthus*	SFZ	— 60.179	— 57.837	806	0.2593	2990	6	382.6	1.6	144.9	0.5	≥*48.6*	0.0005
NBP1103	DH43	Dc-8a	*D. dianthus*	SFZ	— 60.182	— 57.833	823	0.2499	4069	8	6416.5	27.4	149.3	0.9	≥*393.6*	0.0025
NBP1103	**DH43**	**Dc-8b**	***D. dianthus***	**SFZ**	**— 60.182**	**— 57.833**	**823**	**0.1292**	**4122**	**16**	**705.6**	**3.5**	**150.7**	**6.2**	**≥*49.3***	**0.0010**
NBP0805	DR23	Dc-A-1a	*D. dianthus*	SFZ	— 60.182	— 57.834	819	0.4995	4055	13	1555.0	5.4	144.5	0.8	≥*75.6*	0.0044
NBP0805	**DR23**	**Dc-A-1b**[*]	***D. dianthus***	**SFZ**	**— 60.182**	**— 57.834**	**819**	**0.8263**	**4385**	**16**	**2917.0**	**9.2**	**141.5**	**1.0**	**≥*117.2***	**0.0034**
NBP1103	DH43	Dc-3	*D. dianthus*	SFZ	— 60.182	— 57.833	823	0.3599	3208	6	789.8	3.3	146.7	0.5	≥*55.8*	0.0004
NBP0805	DR23	Dc-A-2	*D. dianthus*	SFZ	— 60.182	— 57.834	819	0.4319	4921	16	1032.9	3.6	148.8	0.8	≥*240.6*	0.0060
NBP0805	DR23	Dc-A-3	*D. dianthus*	SFZ	— 60.182	— 57.834	819	0.3797	3472	11	1009.8	3.5	149.5	0.8	≥*136.2*	0.0100
LMG06-05	9	3	*F. curvatum*	B. Bank	— 54.485	— 62.214	318	0.5807	3533	12	21.8	2.6	148.4	0.8	≥*7.3*	0.0002
NBP1103	DH19	Fc-1	*F. curvatum*	B. Bank	— 54.809	— 62.166	1515.5	0.4253	2799	6	994.2	4.3	148.6	0.5	≥*35.4*	0.0003
NBP1103	DH14	Fc-277	*F. curvatum*	B. Bank	—	—	726.5	0.3011	4070	9	682.8	3.0	146.7	0.5	≥*88.8*	0.0005

Table 6 (*continued*)

Cruise	Event	Sample	Species	Location	Lat	Long	Depth (m)	Sample mass (g)	^{238}U (ng/g)	2SE[a]	^{232}Th (pg/g)	2SE	$\delta^{234}U_i$	2SE	Nd (ng/g)	2SE[b]
NBP1103	DH16	Bc-9	*B. malouinensis*	B. Bank	54.713 — 54.808	62.250 — 62.119	1418.5	0.3487	3748	8	2149.2	9.2	148.4	0.6	≥*292.6*	0.0032
NBP1103	DH14	Bn-278	*B. malouinensis*	B. Bank	54.713 — 54.713	62.250 — 62.250	726.5	0.3761	4050	8	481.8	2.0	149.3	0.5	≥*37.8*	0.0004
LMG06-05	9	1	*B. malouinensis*	B. Bank	54.485 — 54.485	62.214 — 62.214	318	0.0921	3683	12	108.1	19.4	151.2	0.7	≥*12.5*	0.0014
NBP1103	DH07	Bn-2	*B. malouinensis*	B. Bank	54.507 — 54.507	62.228 — 62.228	328.5	0.4108	4485	8	287.0	1.3	146.5	0.4	≥*13.9*	0.0003
NBP1103	DH16	Bc-2	*B. malouinensis*	B. Bank	54.808 — 54.808	62.119 — 62.119	1418.5	0.1493	4611	14	552.2	3.6	147.4	4.9	≥*36.5*	0.0009
NBP1103	DH14	Bc-1002	*B. malouinensis*	B. Bank	54.713 — 54.713	62.250 — 62.250	726.5	0.1191	4375	9	1240.7	5.4	148.1	0.5	≥*122.0*	0.0011
NBP1103	DH07	Bn-3	*B. malouinensis*	B. Bank	54.507 — 54.507	62.228 — 62.228	328.5	0.3236	4019	8	422.3	1.9	147.6	0.5	≥*24.7*	0.0004
NBP1103	DH15	Bc-1	*B. malouinensis*	B. Bank	54.772 — 54.772	62.236 — 62.236	894	0.0899	5988	12	1187.9	5.3	145.0	0.5	≥*104.4*	0.0014
NBP1103	DH88	Cc-1a	*Caryophyllia spp.*	Interim	60.560 — 60.560	65.957 — 65.957	982.5	0.2130	3330	6	431.6	1.9	148.5	0.5	≥*90.0*	0.0005
NBP1103	**DH88**	**Cc-1b**	***Caryophyllia spp.***	**Interim**	**60.560 — 60.560**	**65.957 — 65.957**	**982.5**	**0.1691**	**3357**	**6**	**603.3**	**2.7**	**151.4**	**0.5**	**≥*152.1***	**0.0006**
NBP1103	**DH88**	**Cc-1c**	***Caryophyllia spp.***	**Interim**	**60.560 — 60.560**	**65.957 — 65.957**	**982.5**	**0.0703**	**3620**	**14**	**440.3**	**2.7**	**144.6**	**4.4**	**≥*28.5***	**0.0019**
NBP1103	DH75	Gc-4	*G. antarctica*	Interim	60.601 — 60.601	66.002 — 66.002	1195.5	0.0940	6064	12	562.7	2.7	147.0	0.4	≥*118.3*	0.0011
NBP1103	DH75	Gc-3	*G. antarctica*	Interim	60.601 — 60.601	66.002 — 66.002	1195.5	0.1664	5169	10	1046.4	4.5	145.6	0.5	≥*256.7*	0.0007
NBP1103	DH74	Gc-2a	*G. antarctica*	Interim	60.606 — 60.606	66.004 — 66.004	1064	0.1234	4598	9	3495.8	14.7	150.3	0.6	≥*964.5*	0.0054
NBP1103	**DH74**	**Gc-2b**	***G. antarctica***	**Interim**	**60.606 — 60.606**	**66.004 — 66.004**	**1064**	**0.1058**	**4129**	**12**	**2684.5**	**12.6**	**150.8**	**4.3**	**≥*716.7***	**0.0249**

[a] 2SE is the 2σ standard error of the measurement.
[b] 2SE is the propagated 2σ standard error on Nd concentrations determined by isotope dilution.
* Replicates from two aliquots of crushed, but poorly homogenised source sample (see text).
+ Analyses of two corals, one grown on top of the other.
# Re-sampled specimens analysed for Nd isotopes only (accurate Nd concentrations, but no U-Th dating information).

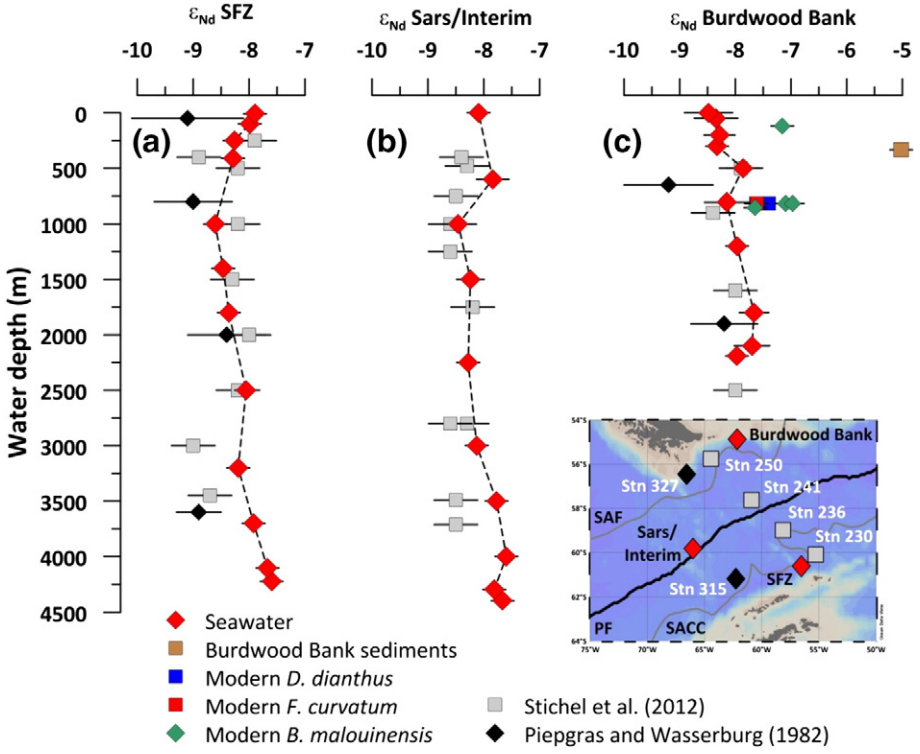

Fig. 5. Drake Passage seawater Nd isotope data. Results from samples collected in May 2008 (this study) are compared to previously published seawater results collected in the area in October 1980 (Piepgras and Wasserburg, 1982) and in April 2008 (Stichel et al., 2012). Inset map illustrates sample locations. Note that stations 241 and 236 from Stichel et al. (2012) have been combined for comparison to the new Sars/Interim profile in panel (b). The Burdwood Bank panel (c) includes modern CWC and sediment Nd isotope data. Abbreviations as in Fig. 1.

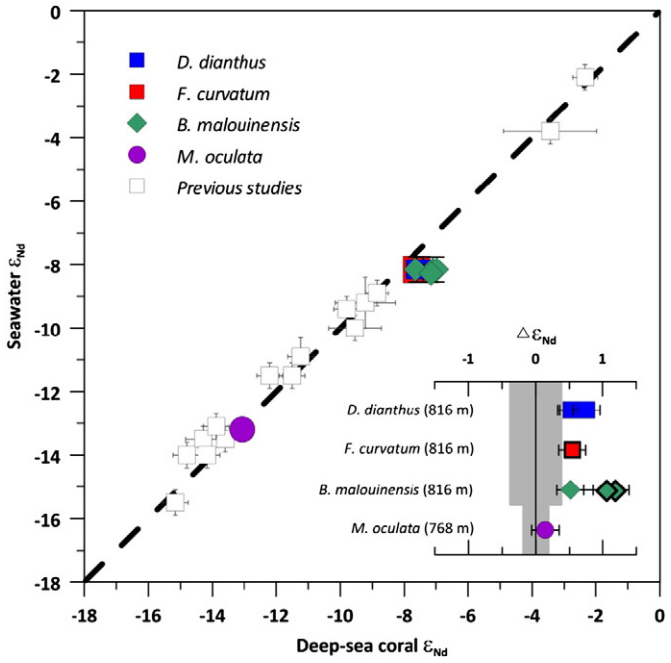

Fig. 6. Global calibration of CWC Nd isotope data and modern seawater. White squares indicate previously published modern calibration data (Copard et al., 2010; van de Flierdt et al., 2010) and coloured symbols are our new results from the Drake Passage (*D. dianthus*, *F. curvatum*, *B. malouinensis*) and the North Atlantic (*M. oculata*). The inset shows the deviation of modern CWC ε_{Nd} from ambient seawater, expressed as $\Delta\varepsilon_{Nd}$ from this study. The grey bar represents the analytical uncertainty of the respective ambient seawater measurement. One *D. dianthus* was replicated within analytical uncertainty (not shown here). Coral specimens collected alive are framed with a thick black line ($n = 3$). All other corals shown in colour were U-Th dated to be ≤467 years old (see text and Table 4 for more details).

Nd/Th ratio of the respective contaminant phase and apply the following equation:

$$\%Nd_{contamination} = \left(\frac{[Th]_{final} \times \left(\frac{[Nd]}{[Th]}\right)_{contaminant}}{[Nd]_{final}} \right) \times 100 \quad (1)$$

The subscript *final* refers to the concentration of the respective element measured in the CWC skeletons. The result for detrital contribution (based on nearby sediment data; Table 3) yields an average contribution to the coral Nd pool of ~3% (for 91 individual analyses), of which 13 samples show values between 5 and 10%. Calculating the same scenario with eq. 1 for other terrigenous elements corroborates this result. For instance, the average Ti-based maximum contribution of terrigeneous Nd to clean coral aragonite samples is ~2% ($n = 16$).

To evaluate the effect of such potential maximum levels of detrital contamination on the Nd isotopic composition of fossil corals, we assume final Nd isotopic compositions of the corals in the range of $\varepsilon_{Nd} = -5.1 \pm 0.2$ to $\varepsilon_{Nd} = -8.4 \pm 0.2$ (Struve, 2016) and use the sediment results reported in Tables 2 and 3:

$$IC_{skeleton} = \frac{IC_{final} \times ([Nd]_{skeleton} \times (1-f_{sed}) + [Nd]_{sed} \times f_{sed}) - (IC_{sed} \times [Nd]_{sed} \times f_{sed})}{([Nd]_{skeleton} \times (1-f_{sed}))} \quad (2)$$

IC in above equation refers to the Nd isotopic composition and *f* to the fraction, the subscripts 'skeleton' to the sediment-free coral skeleton and 'sed' to the sediment-bound Nd fraction, concentration and isotopic composition of the coral skeleton, respectively. The resulting average change in ε_{Nd} is 0.06 units, with seven samples exceeding our typical 2SD external reproducibility of 0.20 ε_{Nd}. These seven samples deviate by 0.22 to 0.45 epsilon units and could be affected by sediment-derived contamination. The largest shift of 0.45 ε_{Nd} is calculated for modern *D. dianthus* NBP0805 TB04 Dp-A-02, which may thus account for the observed (small) offset from ambient seawater values (Fig. 6, Table 4; see above).

The same equations can be used to calculate potential contamination by FeMn oxyhydroxide phases coated onto the coral skeletons. Using a Nd/Th ratio of 2.02 for FeMn coatings on coral skeletons (average of 19 coatings reported by Crocket et al., 2014) and a Nd isotopic composition of $\varepsilon_{Nd} = -7.01 \pm 0.36$ as reported for a 17.1 kyrs BP *D. dianthus* coating collected in 1125 m water depth at Sars seamount (Robinson and van de Flierdt, 2009), the average contribution of FeMn-bound Nd to the coral skeleton Nd budget is 2.1%. This equates to an average shift in Nd isotopic compositions of 0.05 epsilon units ($n = 91$ analyses). Maximum contributions are up to 7.5%, which would result in a correction of 0.34 ε_{Nd}. However, only three samples, one of which is modern NBP0805 TB04 Dp-A-02, would experience a shift in excess of the external reproducibility of 0.20 ε_{Nd}.

In summary, the only way to create an isotopic effect from detrital or FeMn contaminant phases in our fossil coral data set from the Drake Passage is to assume no ^{232}Th in pure authigenic aragonite, linear coupling of Nd and ^{232}Th, and 100% sourcing of ^{232}Th from the respective contaminant phase. These assumptions are purposely extreme, but still reveal that only a small number of corals would be affected by contamination-induced shifts in their Nd isotopic composition by up to 0.45 epsilon units. We hence conclude that interpretations of shifts in excess of this signal are robust for the Nd and ^{232}Th concentration ranges observed. We however note that a ^{232}Th-based correction may in fact overcorrect, as ^{232}Th can also be concentrated from seawater during coral growth (e.g., Cheng et al., 2000; Spooner et al., 2016). This calls for an authigenic (seawater-derived) Nd carrier phase causing the enrichment of Nd within the aragonitic skeletons.

5.2.2. Rare earth element case for a seawater origin

Further support for an insignificant role of Nd contamination by detritus and FeMn coatings on fully cleaned fossil and modern CWC aragonite comes from shale-normalised REE patterns (Table 5, Fig. 8). Local sediments show relatively flat REE patterns, with no notable Ce anomaly, and a slight enrichment in HREE over LREE. FeMn coatings reported by Crocket et al. (2014 and pers. comm.) show relatively flat patterns with a positive Ce anomaly and a slight enrichment of mid-REE (Fig. 8). In contrast, all results obtained from modern and fossil CWCs ($n = 17$) show pronounced negative Ce anomalies. Given the low concentrations of Ce in coral aragonite, contamination from FeMn coatings and/or lithogenic sources should be readily detectable by a less pronounced Ce anomaly, which is however not the case (Figs. 7 and 8, Table 5). Moreover, stabilities of aqueous REE carbonate complexes in seawater increase with increasing atomic numbers resulting in characteristic HREE enrichment in seawater (e.g., De Baar et al., 1985; Cantrell and Byrne, 1987; Byrne and Li, 1995), and hence in CDW (Hathorne et al., 2015; Fig. 8). The same features can be observed in CWC aragonite, even for the species *B. malouinensis* and *G. antarctica*, which showed suspicious co-variation of [Nd] and [^{232}Th]. We conclude that the Nd in excess of predicted coral [Nd] from inorganic aragonite precipitation experiments seems authigenic in nature. Authigenic (secondary) calcite can concentrate REE from seawater. However, the REE enrichment from inorganic calcite co-precipitation is similar to aragonite (Terakado and Masuda, 1988), and even the elevated concentrations in cleaned foraminiferal calcite are too low to significantly enrich REE as a minor component in the coral skeleton (e.g., Palmer, 1985; Haley et al., 2005; Roberts et al., 2012; Fig. 8).

5.2.3. Organic phases as potential Nd carrier in coral skeletons

The skeletons of SWC and CWC are characterised by microstructures that feature an area where biologically mediated precipitation happens, referred to as centres of calcification (COC), a chemically and morphologically distinct area of surrounding fibrous aragonite (e.g., Cuif and

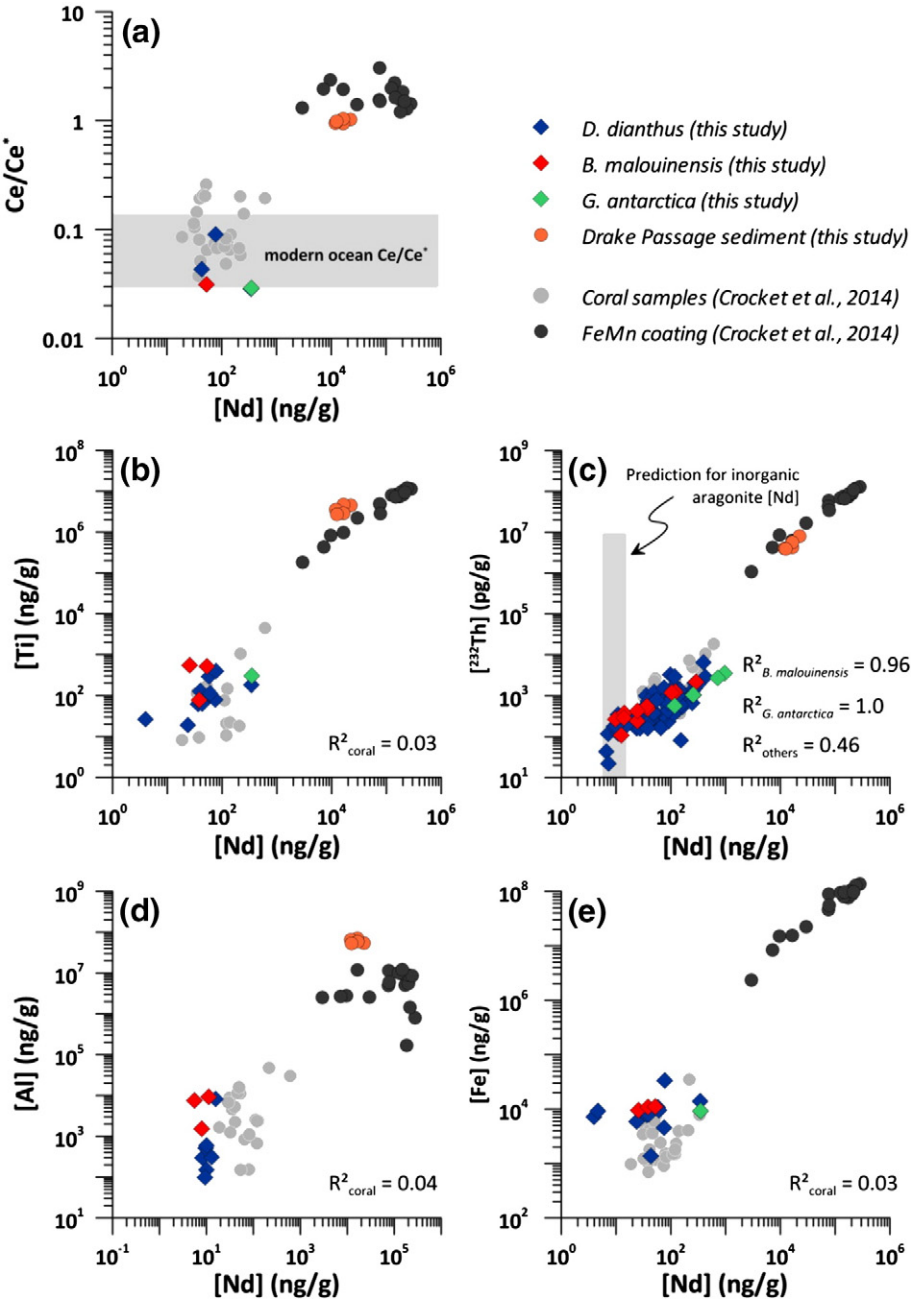

Fig. 7. Drake Passage CWC and sediment trace metal data. All results, except for Nd concentrations in panel (c), are derived from ICP-MS analyses of resampled corals. Coral and FeMn coating results by Crocket et al. (2014) are included for comparison. (a) [Nd] vs. Ce/Ce*; $Ce/Ce^* = 2 \times Ce_N / (La_N + Pr_N)$; modern deep ocean Ce/Ce* from Hathorne et al. (2015, and references therein). (b) [Nd] vs. [Ti], (c) Drake Passage coral ^{232}Th (Burke and Robinson, 2012; Chen et al., 2015; Burke et al., unpubl. data; Tables 4 and 6) and Nd concentrations are based on isotope dilution so that Drake Passage coral Nd concentrations are minimum estimates (see text and Tables 4 and 6 for further information). All other Nd concentrations are accurate. Linear correlation coefficient for [Nd] vs. [^{232}Th] for all corals: $R^2 = 0.48$ ($n = 91$). Higher coefficients are found when considering only *B. malouinensis* ($R^2 = 0.96$, $n = 11$), and *G. antarctica* ($R^2 = 1$, $n = 4$). Grey bar indicates predicted $[Nd]_{coral}$ calculated from inorganic precipitation K_D value 4.3 (Terakado and Masuda, 1988) assuming a $[Nd]_{seawater}$ range of 10–19 pmol/kg, based on concentration data for Drake Passage seawater from Stichel et al. (2012). (d) [Nd] vs. [Al]. (e) [Nd] vs. [Fe], no sediment Fe data available.

Dauphin, 1998; Adkins et al., 2003; Cuif et al., 2003). These COCs are characterised by high abundances of organic molecules, i.e., sugars and amino acids that mediate the formation of amorphous aragonite precursor phases, associated with strong chemical heterogeneity (e.g., Cuif and Dauphin, 1998, 2005; Cuif et al., 2003; Stolarski, 2003; Montagna et al., 2005, 2014; Dauphin et al., 2006; Helman et al., 2008; Przeniosło et al., 2008; Brahmi et al., 2010; Anagnostou et al., 2011).

The concentration of some trace elements can be enhanced in COCs, i.e., areas where organics are enriched (cf. e.g., Cuif and Dauphin, 1998; Cuif et al., 2003; Montagna et al., 2005; Case et al., 2010; Anagnostou et al., 2011; Rollion-Bard and Blamart, 2015). Other trace elements, including Th and U, however, seem depleted in such areas of rapid calcification (e.g., Robinson et al., 2006; Sinclair et al., 2006; Brahmi et al., 2010; Anagnostou et al., 2011; Spooner et al., 2016). Cheng et al. (2000) found high ^{232}Th concentrations associated with exposed organic material scraped off the aragonitic skeletons of *D. dianthus* specimens. Anagnostou et al. (2011) ascribed regions of elevated Fe/Ca and Mn/Ca in covariation with P/Ca along a septum of CWC *D. dianthus* to FeMn oxyhydroxides. Such covariation with P/Ca may alternatively be related to organic compounds causing enhanced surface sorption of Fe and Mn from ambient seawater, which could be incorporated into the coral skeleton during ongoing growth. Indeed, Anagnostou et al. (2011) consider

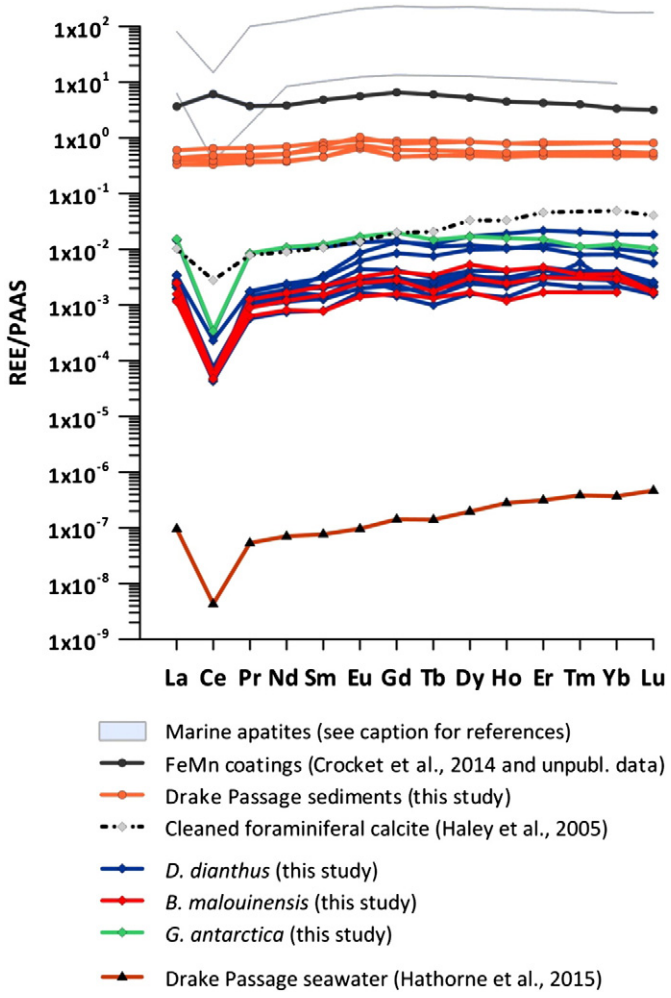

Fig. 8. Shale-normalised REE data. Sedimentary REE patterns from locations across the Drake Passage (see Fig. 2 for locations) and average values for FeMn coating data from North Atlantic CWCs (n = 18; Crocket et al., 2014, and Crocket, 2015 pers. communication). CWC REE results for a selected group of modern and fossil samples (see Table 5). Due to the low concentrations of REE in clean coral aragonite low abundance elements like Ce, Tm and Lu were below the limit of detection in some samples (Table 5). For visualisation purposes we used the REE concentration of the detection limit to calculate shale-normalised Ce values (Taylor and McLennan, 1985). Samples NBP0805 TB04 Big Beauty and NBP0805 DR35 Dc-A1 yielded very low REE concentrations overall (Table 5), and were hence not included in the Figure. Marine apatite data with seawater-like REE patterns from the North Pacific (high and low REE mud from Kon et al., 2014), Southern Ocean ODP site 689 (Martin et al., 2010) and from Cape Basin 9940K and 9942 samples (Elderfield and Pagett, 1986). Cleaned foraminiferal calcite data (*G. sacculifer*) from Southeast Pacific 54MC coretop (Haley et al., 2005). Seawater data from Drake Passage CDW is from 1250 m water depth at Stn 241 in Hathorne et al. (2015). See caption of Table 3 for PAAS values used for shale-normalisation.

organic phosphorus in *D. dianthus* skeletons significant and organics mediate cyclic inter- and intra-crystal growth and the orientation of aragonitic fibres on micron to nano-scale (e.g., Cuif et al., 1999, 2003; Stolarski, 2003; Helman et al., 2008; Przeniosło et al., 2008; Webb et al., 2009). Inner-skeletal organics thus appear a potential candidate to elevate Nd concentrations. Furthermore, the heterogeneous distribution of organic compounds in the coral skeleton could perhaps account for some of the intraskeletal Nd variability as evident from the large range of Nd concentrations in resampled coral pieces.

Stanley and Byrne (1990) conducted exposure experiments on the living algae *Ulva lactuca* to test partitioning of REE between aqueous and marine organic phases. For exposure times of 6 h at pH = 7.5 and pCO_2 = 329 μmol/mol they found solid-solution partitioning ($[REE]_{organics}/[REE]_{seawater}$) of ~980 for Ce and ~1850 for Eu and a decrease with increasing pH. Using the higher Eu value of 1850 with observed seawater Nd concentrations in the Drake Passage of up to 30.09 pmol/kg (Stichel et al., 2012), a Nd concentration in organic phases of ~8 ng/g can be calculated. Following the estimate from Cuif et al. (2004) that the overall proportion of organics in scleractinian SWC and CWC skeletons is ~2.5 wt%, the maximum contribution of organic-bound Nd to the coral Nd budget would be ~0.2 ng/g corresponding to <3% of the skeletal Nd. The life cycle of a coral is however orders of magnitude longer than 6 h (*D. dianthus*: ~100 years; Adkins et al., 2004). Organic compounds exposed to seawater may accumulate Nd until the functional groups are saturated thus enriching Nd similar to foraminifera (Vance et al., 2004; Martínez-Botí et al., 2009). However, evidence from the Gd anomalies ($Gd/Gd^* = 2 \times Gd_N / (Eu_N + Tb_N)$) in our corals does not support the idea of a dominant role of organics for the coral REE budget. If the REE budget were controlled by organic scavenging from seawater the Gd anomaly should be negative (Byrne and Kim, 1990; Lee and Byrne, 1993). The average Gd/Gd^*_{coral} is however 1.2 ± 0.1 (n = 15; Table 5), i.e., slightly positive, and rather resembles Drake Passage UCDW Gd anomalies, which are also slightly positive ($Gd/Gd^* \approx 1.3$; Hathorne et al., 2015).

5.2.4. Phosphate phases as Nd carrier in coral skeletons

Another authigenic phase previously considered in coral aragonite and capable of concentrating seawater REE are phosphates like apatite (Montagna et al., 2006; LaVigne et al., 2010; Mason et al., 2011). Anagnostou et al. (2011) showed that ferric phosphate is not occurring in *D. dianthus* skeletons. Mason et al. (2011) investigated septae and thecae of modern and fossil *D. dianthus*, *Flabellum* sp. and *Lophelia pertusa* specimens from various marine environments. A combination of laser-ablation ICP-MS, solid-state NMR (nuclear magnetic resonance) spectroscopy and solution ICP-MS was used to identify hydroxyapatite as a significant phosphate-hosting mineral in coral skeletons (Mason et al., 2011). Concentrations of hydroxyapatite were found to be highly variable between individual samples, independent of environmental factors such as dissolved inorganic phosphate or depth, and were not related to bulk coral phosphate content or preservation state (Mason et al., 2011). While surficial apatite would be removed during the cleaning procedure, hydroxyapatite inclusions in the coral skeletons could remain unaffected by the cleaning procedure, and probably widely insensitive to diagenesis. It is very likely that such inclusions would be enriched in seawater-derived REE (i.e., by analogy to biogenic apatite like fish teeth; Elderfield and Pagett, 1986; Martin et al., 2010) and thus capable of creating the large observed range of Nd concentrations within and between fossil and modern CWC specimens.

The maximum solid-bound P in coral skeletons was found to be 319 ± 79 μg/g, of which up to 41 ± 7% are estimated to be apatite-bound (Mason et al., 2011). Hydroxyapatite has the formula $Ca_5(PO_4)_3(OH)$, in which P accounts for 92.9 of the 502.3 amu, yielding a P/apatite ratio of 0.185 and a P-based maximum estimate of ~707 μg/g of apatite in coral aragonite. Fish teeth are known to contain seawater-like REE patterns and Nd concentrations of up to 1460 μg/g (e.g., Elderfield and Pagett, 1986; Martin et al., 2010). Using this estimate as upper limit for $[Nd]_{apatite}$ translates to ~1 μg apatite-bound Nd per g of coral skeleton. This calculated value is in excellent agreement with the highest Nd concentrations observed in our entire set of fossil and modern corals (i.e., $[Nd_{min}]$ = 964.5 ng/g; Tables 4 and 6) and a prominent role of apatite for the skeletal Nd budget is consistent with similar P/Nd ratios of ~130 in coral skeletons and authigenic apatite (fish teeth), respectively. Although it awaits confirmation from direct evidence through microsampling techniques, our trace metal data is consistent with this hypothesis.

Formation of authigenic and/or biogenic P-rich phases, presumably apatite included in the coral skeletons could have a major impact on the Nd budget, without affecting some other elemental concentrations. For example, U concentrations in fish teeth are 0.7–11 μg/g (Baturin, 2001), similar to the U concentrations in clean CWC aragonite (e.g., Cheng et al., 2000; Table 6). Concentrations of Nd in fish teeth are up

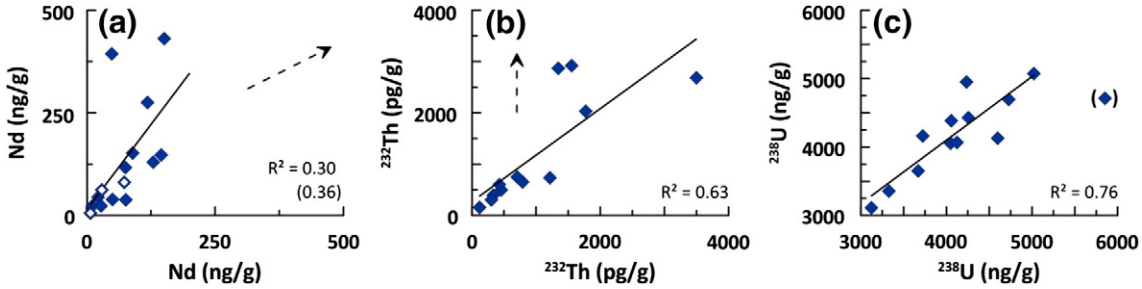

Fig. 9. Trace metal results of different subsamples of the same coral. Dark blue diamonds represent Nd, Th and U data obtained from isotope dilution, i.e., in panel (a) [Nd_{min}] (<12% Nd loss), and the white diamonds with blue outline are [Nd_{min}] plotted against accurate Nd concentrations (y-axis) of different subsamples of the same coral (Tables 4 and 6; see text for details). The correlation coefficients were generated by omitting one outlier, which is pointed towards by the dashed arrow in panels (a) (NBP1103 DH74 Gc-2a/b) and (b) (NBP1103 DH43 Dc-8a/b) and displayed in brackets in panel (c). Including the pairs of minimum vs. accurate Nd concentration data in panel (a) increases the linear R^2 to 0.36 (in brackets). For corals NBP1103 DH88 Cc-1 and NBP0805 DR35 Dc-E-1 subsamples 'a' and 'b' were chosen for correlation, respectively.

to 1460 μg/g (Elderfield and Pagett, 1986) and are thus about one order of magnitude higher than in coral skeletons yielding consequently high Nd/U of ~133 to 2086 in fish teeth (cf. e.g., Cheng et al., 2000; Baturin, 2001; Crocket et al., 2014; this study). Therefore, the effect of heterogeneously distributed apatite inclusions on coral [^{238}U] is presumably limited. This observation is supported by relatively good reproducibility of [^{238}U] ($R^2 = 0.76$), but also [^{232}Th] ($R^2 = 0.63$), from different subsamples of the same coral specimen, while [Nd_{min}] reproduce poorly (i.e., more heterogeneous; $R^2 = 0.30$ (0.36); Fig. 9). Indeed, the inner-skeletal distributions of ^{238}U and ^{232}Th are strongly influenced by the skeletal microstructures (e.g., Robinson et al., 2006; Sinclair et al., 2006; LaVigne et al., 2010; Anagnostou et al., 2011; Raddatz et al., 2014; Spooner et al., 2016). Sampling such microstructures to different degrees could hence influence trace metal concentrations in individual coral subsamples. Such sampling bias should be expressed by covariations between the reproducibility of replicate U, Th and Nd concentrations, and sample size. Calculating the deviation of U, Th and Nd_{min} concentrations between different subsamples from the same coral ($n = 12$, selected as for Fig. 9) reveals only for Nd a correspondence of reduced deviation with larger sample size ($R^2 = 0.30$; indicator for sample size: mean mass of the subsamples per coral). This trend is however dominated by a strong covariation in the mass range below 0.2 g and diminishes for subsamples above ~0.2 g weight. The reason for this effect is presumably related to higher susceptibility of particularly small subsamples to skeletal heterogeneity and/or to contaminant phases. Therefore, the trends in our U, Th and Nd concentration data are unlikely to be introduced by a sampling bias.

It is thus proposed that apatite inclusions can be an important carrier phase of Nd in CWC skeletons, a hypothesis to be verified by future work. However, experimental studies showed that a slight depletion in HREE in coral aragonite, compared to seawater, is controlled by the combined effect of sorption onto hydroxyapatite surfaces (i.e., K_D decrease towards HREE: Koeppenkastrop and De Carlo, 1992) and quantitative assimilation of the REE from ambient seawater (i.e., no fractionation during incorporation; Reynard et al., 1999). Overall, the large variability of major and trace element concentrations in apatite is consistent with the observed difficulty to reproduce coral Nd concentrations (Fig. 9) as well as the fact that different individual locations, such as the Northwest Atlantic (Crocket et al., 2014), the Northeast Atlantic (Colin et al., 2010; Copard et al., 2011, 2012; Montero-Serrano et al., 2013), and the Drake Passage (this study), all show large ranges of coral Nd concentrations, even though contaminant phases are shown to exert only a very limited effect on the budgets of rigorously cleaned coral aragonite.

6. Conclusions

We presented new data that expand on the existing modern calibration of CWC aragonite as an archive for seawater Nd isotopes. By comparing alive-collected and recently dead corals of the species *F. curvatum* and *D. dianthus* from the Drake Passage with ambient seawater, we confirm that these species are robust seawater Nd isotope archives. A similar conclusion can be reached for the species *M. oculata* based on new results from the North Atlantic. Of the species *B. malouinensis*, however, two of the three specimens investigated with closed U system behaviour do not match modern seawater Nd isotopic composition. Data from this species should be interpreted with caution until further studies (e.g., on growth rate or in combination with pore waters) become available.

Despite the good agreement in Nd isotopic compositions of modern coral specimens with ambient seawater signatures, this study confirms earlier findings that Nd concentrations in coral aragonite can be significantly elevated over that expected from inorganic precipitation experiments. Modern and fossil coral skeletons furthermore reveal variability in Nd concentrations of up to two orders of magnitude. Mass balance considerations using new results from local sediments, as well as previously published results on ferromanganese oxyhydroxide precipitates, rule out major contributions from these phases. Seawater-like REE patterns in corals provide strong evidence for nearly unfractionated uptake of REE from ambient seawater. We here suggest that apatite inclusions can be a significant carrier-phase concentrating ambient REE from the dissolved phase. Thus fossil CWC skeletons are not compromised as robust recorders of seawater Nd isotopic composition, despite variable Nd concentrations.

Acknowledgements

We acknowledge Rhian Waller, Kathryn Scanlon and the science team and crews of CE0806, LMG0506, NBP0805 and NBP1103 for collecting and supplying sample material. Katharina Kreissig and Barry Coles are thanked for their help with laboratory analyses. Tianyu Chen is thanked for comments on an earlier version of the manuscript and Ana Samperiz for taking coral photos. TvdF and TS acknowledge financial support for a bursary by the Grantham Institute of Climate Change and the Environment and a Marie Curie Reintegration grant (IRG 230828), as well as funding from the Leverhulme Trust (RPG-398) and the NERC (NE/N001141/1). Additional financial support was provided to LFR by the USGS-WHOI Co-operative agreement, NSF-ANT grants 0636787 and 80295700, The European Research Council, the Leverhulme Trust and a Marie Curie Reintegration grant. LB was supported by a NOAA/UCAR Climate and Global Change Postdoctoral Fellowship and KJM acknowledges funding from a Marie Curie International Outgoing fellowship (IOF 236962). We thank Michael E. Böttcher for editorial handling and two anonymous reviewers for their helpful comments on the manuscript.

References

Abbott, A.N., Haley, B.A., McManus, J., Reimers, C.E., 2015. The sedimentary flux of dissolved rare earth elements to the ocean. Geochim. Cosmochim. Acta 154:186–200. http://dx.doi.org/10.1016/j.gca.2015.01.010.

Addamo, A.M., Vertino, A., Stolarski, J., García-Jiménez, R., Taviani, M., Machordom, A., 2016. Merging scleractinian genera: the overwhelming genetic similarity between solitary Desmophyllum and colonial Lophelia. BMC Evol. Biol. 16:108–125. http://dx.doi.org/10.1186/s12862-016-0654-8.

Adkins, J.F., Cheng, H., Boyle, E.A., Druffel, E.R.M., Edwards, R.L., 1998. Deep-sea coral evidence for rapid change in ventilation of the deep North Atlantic 15,400 years ago. Science 280:725–728. http://dx.doi.org/10.1126/science.280.5364.725.

Adkins, J.F., Boyle, E.A., Curry, W.B., Lutringer, A., 2003. Stable isotopes in deep-sea corals and a new mechanism for "vital effects". Geochim. Cosmochim. Acta 67:1129–1143. http://dx.doi.org/10.1016/S0016-7037(02)01203-6.

Adkins, J.F., Henderson, G.M., Wang, S.-L., O'Shea, S., Mokadem, F., 2004. Growth rates of the deep-sea scleractinia *Desmophyllum cristagalli* and *Enallopsammia rostrata*. Earth Planet. Sci. Lett. 227:481–490. http://dx.doi.org/10.1016/j.epsl.2004.08.022.

Akagi, T., Hashimoto, Y., F-F, F., Tsuno, H., Tao, H., Nakano, Y., 2004. Variation of the distribution coefficients of rare earth elements in modern coral-lattices: species and site dependencies. Geochim. Cosmochim. Acta 68:2265–2273. http://dx.doi.org/10.1016/j.gca.2003.12.014.

Anagnostou, E., Sherrell, R.M., Gagnon, A., LaVigne, M., Field, M.P., McDonough, W.F., 2011. Seawater nutrient and carbonate ion concentrations recorded as P/Ca, Ba/Ca, and U/Ca in the deep-sea coral *Desmophyllum dianthus*. Geochim. Cosmochim. Acta 75:2529–2543. http://dx.doi.org/10.1016/j.gca.2011.02.019.

Andersen, M.B., Stirling, C.H., Zimmermann, B., Halliday, A.N., 2010. Precise determination of the open ocean 234U/238U composition. Geochem. Geophys. Geosyst. 11, Q12003. http://dx.doi.org/10.1029/2010GC003318.

Andreasen, R., Sharma, M., 2009. Fractionation and mixing in a thermal ionization mass spectrometer source: implications and limitations for high-precision Nd isotope analyses. Int. J. Mass Spectrom. 285:49–57. http://dx.doi.org/10.1016/j.ijms.2009.04.004.

Auro, M.E., Robinson, L.F., Burke, A., Bradtmiller, L.I., Fleisher, M.Q., Anderson, R.F., 2012. Improvements to 232-thorium, 230-thorium, and 231-protactinium analysis in seawater arising from GEOTRACES intercalibration. Limnol. Oceanogr. Methods 10 (7): 464–474. http://dx.doi.org/10.4319/lom.2012.10.464.

Basak, C., Pahnke, K., Frank, M., Lamy, F., Gersonde, R., 2015. Neodymium isotopic characterization of Ross Sea bottom water and its advection through the southern South Pacific. Earth Planet. Sci. Lett. 419:211–221. http://dx.doi.org/10.1016/j.epsl.2015.03.011.

Baturin, G.N., 2001. Uranium and thorium in phosphatic bone debris from the ocean bottom. Lithol. Miner. Resour. 36 (2):99–108. http://dx.doi.org/10.1023/A:1004866215497.

Bau, M., Koschinsky, A., Dulski, P., Hein, J.R., 1996. Comparison of the partitioning behaviours of yttrium, rare earth elements, and titanium between hydrogenetic marine ferromanganese crusts and seawater. Geochim. Cosmochim. Acta 60:1709–1725. http://dx.doi.org/10.1016/0016-7037(96)00063-4.

Brahmi, C., Meibom, A., Smith, D.C., Stolarski, J., Auzoux-Bordenave, S., Nouet, J., Doumenc, D., Djediat, C., Domart-Coulon, I., 2010. Skeletal growth, ultrastructure and composition of the azooxanthellate scleractinian coral *Balanophyllia regia*. Coral Reefs 29: 175–189. http://dx.doi.org/10.1007/s00338-009-0557-x.

Brearley, J.A., Sheen, K.L., Naveira Garabato, A.C., Smeed, D.A., Speer, K.G., Thurnherr, A.M., Meredith, M.P., Waterman, S., 2014. Deep boundary current disintegration in Drake Passage. Geophys. Res. Lett. 41, 2013GL058617. http://dx.doi.org/10.1002/2013GL058617.

Burke, A., Robinson, L.F., McNichol, A.P., Jenkins, W.J., Scanlon, K.M., Gerlach, D.S., 2010. Reconnaissance dating: A new radiocarbon method applied to assessing the temporal distribution of Southern Ocean deep-sea corals. Deep Sea Res., Part I 57:1510–1520. http://dx.doi.org/10.1016/j.dsr.2010.07.010.

Burke, A., 2012. Constraining Circulation Changes Through the Last Deglaciation With Deep-sea Coral Radiocarbon and Sedimentary 231Pa/230Th (PhD thesis). (MIT/WHOI).

Burke, A., Robinson, L.F., 2012. The Southern Ocean's role in carbon exchange during the last deglaciation. Science 335:557–561. http://dx.doi.org/10.1126/science.1208163.

Byrne, R.H., Kim, K.-H., 1990. Rare earth element scavenging in seawater. Geochim. Cosmochim. Acta 54:2645–2656. http://dx.doi.org/10.1016/0016-7037(90)90002-3.

Byrne, R.H., Li, B., 1995. Comparative complexation behavior of the rare earths. Geochim. Cosmochim. Acta 59:4575–4589. http://dx.doi.org/10.1016/0016-7037(95)00303-7.

Cairns, S.D., 1982. Antarctic and Subantarctic Scleractinia. In: Kornicker, L.S. (Ed.)Antarctic Research Series 34. American Geophysical Union:pp. 1–74 (available from: http://dx.doi.org/10.1029/AR034p0001).

Cairns, S.D., Häussermann, V., Försterra, G., 2005. A review of the Scleractinia (Cnidaria: Anthozoa) of Chile, with the description of two new species. Zootaxa 1018, 15–46.

Cairns, S.D., Kitahara, M.V., 2012. An illustrated key to the genera and subgenera of the recent azooxanthellate Scleractinia (Cnidaria, Anthozoa), with an attached glossary. ZooKeys 227:1–47. http://dx.doi.org/10.3897/zookeys.227.3612.

Cantrell, K.J., Byrne, R.H., 1987. Rare earth element complexation by carbonate and oxalate ions. Geochim. Cosmochim. Acta 51:597–605. http://dx.doi.org/10.1016/0016-7037(87)90072-X.

Carter, P., Vance, D., Hillenbrand, C.D., Smith, J.A., Shoosmith, D.R., 2012. The neodymium isotopic composition of waters masses in the eastern Pacific sector of the Southern Ocean. Geochim. Cosmochim. Acta 79:41–59. http://dx.doi.org/10.1016/j.gca.2011.11.034.

Case, D.H., Robinson, L.F., Auro, M.E., Gagnon, A.C., 2010. Environmental and biological controls on Mg and Li in deep-sea scleractinian corals. Earth Planet. Sci. Lett. 300 (3–4):215–225. http://dx.doi.org/10.1016/j.epsl.2010.09.029.

Chabaux, F., Unions, R.K., Cohen, A.S., Hein, J.R., 1997. 238U234U230Th disequilibrium in hydrogenous oceanic FeMn crusts: palaeoceanographic record or diagenetic alteration? Geochim. Cosmochim. Acta 61:3619–3632. http://dx.doi.org/10.1016/S0016-7037(97)00187-7.

Chen, T., Robinson, L.F., Burke, A., Southon, J., Spooner, P., Morris, P.J., Ng, H.C., 2015. Synchronous centennial abrupt events in the ocean and atmosphere during the last deglaciation. Science 349:1537–1541. http://dx.doi.org/10.1126/science.aac6159.

Cheng, H., Adkins, J., Edwards, R.L., Boyle, E.A., 2000. U-Th dating of deep-sea corals. Geochim. Cosmochim. Acta 64:2401–2416. http://dx.doi.org/10.1016/S0016-7037(99)00422-6.

Cochran, J.K., Carey, A.E., Sholkovitz, E.R., Surprenant, L.D., 1986. The geochemistry of uranium and thorium in coastal marine sediments and sediment pore waters. Geochim. Cosmochim. Acta 50:663–680. http://dx.doi.org/10.1016/0016-7037(86)90344-3.

Colin, C., Frank, N., Copard, K., Douville, E., 2010. Neodymium isotopic composition of deep-sea corals from the NE Atlantic: implications for past hydrological changes during the Holocene. Quat. Sci. Rev. 29:2509–2517. http://dx.doi.org/10.1016/j.quascirev.2010.05.012.

Cook, C.P., van de Flierdt, T., Williams, T., Hemming, S.R., Iwai, M., Kobayashi, M., Jimenez-Espejo, F.J., Escutia, C., Gonzalez, J.J., Khim, B.-K., McKay, R.M., Passchier, S., Bohaty, S.M., Riesselman, C.R., Tauxe, L., Sugisaki, S., Galindo, A.L., Patterson, M.O., Sangiorgi, F., Pierce, E.L., Brinkhuis, H., Klaus, A., Fehr, A., Bendle, J.A.P., Bijl, P.K., Carr, S.A., Dunbar, R.B., Flores, J.A., Hayden, T.G., Katsuki, K., Kong, G.S., Nakai, M., Olney, M.P., Pekar, S.F., Pross, J., Rohl, U., Sakai, T., Shrivastava, P.K., Stickley, C.E., Tuo, S., Welsh, K., Yamane, M., 2013. Dynamic behaviour of the East Antarctic ice sheet during Pliocene warmth. Nat. Geosci. 6:765–769. http://dx.doi.org/10.1038/ngeo1889.

Copard, K., Colin, C., Douville, E., Freiwald, A., Gudmundsson, G., De Mol, B., Frank, N., 2010. Nd isotopes in deep-sea corals in the North-eastern Atlantic. Quat. Sci. Rev. 29:2499–2508. http://dx.doi.org/10.1016/j.quascirev.2010.05.025.

Copard, K., Colin, C., Frank, N., Jeandel, C., Montero-Serrano, J.-C., Reverdin, G., Ferron, B., 2011. Nd isotopic composition of water masses and dilution of the Mediterranean outflow along the southwest European margin. Geochem. Geophys. Geosyst. 12, Q06020. http://dx.doi.org/10.1029/2011GC003529.

Copard, K., Colin, C., Henderson, G.M., Scholten, J., Douville, E., Sicre, M.-A., Frank, N., 2012. Late Holocene intermediate water variability in the northeastern Atlantic as recorded by deep-sea corals. Earth Planet. Sci. Lett. 313–314:34–44. http://dx.doi.org/10.1016/j.epsl.2011.09.047.

Crocket, K.C., Lambelet, M., van de Flierdt, T., Rehkämper, M., Robinson, L.F., 2014. Measurement of fossil deep-sea coral Nd isotopic compositions and concentrations by TIMS as NdO+, with evaluation of cleaning protocols. Chem. Geol. 374–375: 128–140. http://dx.doi.org/10.1016/j.chemgeo.2014.03.011.

Cuif, J.-P., Dauphin, Y., 1998. Microstructural and physico-chemical characterization of 'centers of calcification' in septa of some recent scleractinian corals. Paläontol. Z. 72:257–269. http://dx.doi.org/10.1007/BF02988357.

Cuif, J.-P., Dauphin, Y., Gautret, P., 1999. Compositional diversity of soluble mineralizing matrices in some recent coral skeletons compared to fine-scale growth structures of fibres: discussion of consequences for biomineralization and diagenesis. Int. J. Earth Sci. 88:582–592. http://dx.doi.org/10.1007/s005310050286.

Cuif, J.-P., Dauphin, Y., Doucet, J., Salome, M., Susini, J., 2003. XANES mapping of organic sulfate in three scleractinian coral skeletons. Geochim. Cosmochim. Acta 67:75–83. http://dx.doi.org/10.1016/S0016-7037(02)01041-4.

Cuif, J.-P., Dauphin, Y., Berthet, P., Jegoudez, J., 2004. Associated water and organic compounds in coral skeletons: quantitative thermogravimetry coupled to infrared absorption spectrometry. Geochem. Geophys. Geosyst. 5, Q11011. http://dx.doi.org/10.1029/2004GC000783.

Cuif, J.P., Dauphin, Y., 2005. The environment recording unit in coral skeletons - a synthesis of structural and chemical evidences for a biochemically driven, stepping-growth process in fibres. Biogeosciences 2:61–73. http://dx.doi.org/10.5194/bg-2-61-2005.

[dataset]Dalziel, I., 2015. Calibrated Hydrographic Data From Drake Passage Acquired With a CTD During the Nathaniel B. Palmer Expedition NBP0805 (2008), Integrated Earth Data Applications (IEDA). http://doi.org/10.1594/IEDA/313716.

Dauphin, Y., Cuif, J.-P., Massard, P., 2006. Persistent organic components in heated coral aragonitic skeletons—implications for palaeoenvironmental reconstructions. Chem. Geol. 231:26–37. http://dx.doi.org/10.1016/j.chemgeo.2005.12.010.

De Baar, H.J.W., Bacon, M.P., Brewer, P.G., Bruland, K.W., 1985. Rare earth elements in the Pacific and Atlantic Oceans. Geochim. Cosmochim. Acta 49:1943–1959. http://dx.doi.org/10.1016/0016-7037(85)90089-4.

Edwards, R., Chen, J.H., Wasserburg, G.J., 1987. 238U234U230Th232Th systematics and the precise measurement of time over the past 500,000 years. Earth Planet. Sci. Lett. 81:175–192. http://dx.doi.org/10.1016/0012-821X(87)90154-3.

Elderfield, H., Greaves, M.J., 1982. The rare earth elements in seawater. Nature 296 (5854):214–219. http://dx.doi.org/10.1038/296214a0.

Elderfield, H., Pagett, R., 1986. Rare earth elements in ichthyoliths: variations with redox conditions and depositional environment. Sci. Total Environ. 49:175–197. http://dx.doi.org/10.1016/0048-9697(86)90239-1.

Frank, N., Paterne, M., Ayliffe, L., van Weering, T., Henriet, J.-P., Blamart, D., 2004. Eastern North Atlantic deep-sea corals: tracing upper intermediate water Δ14C during the Holocene, Earth Planet. Earth Planet. Sci. Lett. 219:297–309. http://dx.doi.org/10.1016/S0012-821X(03)00721-0.

Garcia, H.E., Locarnini, R.A., Boyer, T.P., Antonov, J.I., Baranova, O.K., Zweng, M.M., Reagan, J.R., Johnson, D.R., 2013. World Ocean Atlas 2013. In: Levitus, S., Mishonov, A. (Eds.), Volume 3: Dissolved Oxygen, Apparent Oxygen Utilization, and Oxygen Saturation 75. NOAA Atlas NESDIS Technical Ed. (27 pp).

Gass, S.E., Roberts, J.M., 2006. The occurrence of the cold-water coral *Lophelia pertusa* (Scleractinia) on oil and gas platforms in the North Sea: colony growth, recruitment and environmental controls on distribution. Mar. Pollut. Bull. 52:549–559. http://dx.doi.org/10.1016/j.marpolbul.2005.10.002.

GEOROC database: http://georoc.mpch-mainz.gwdg.de/georoc/

Hamel, J.F., Sun, Z., Mercier, A., 2010. Influence of size and seasonal factors on the growth of the deep-sea coral *Flabellum alabastrum* in mesocosm. Coral Reefs 29:521–525. http://dx.doi.org/10.1007/s00338-010-0590-9.

Hathorne, E.C., Stichel, T., Brück, B., Frank, M., 2015. Rare earth element distribution in the Atlantic sector of the Southern Ocean: the balance between particle scavenging and vertical supply. Mar. Chem. 177:157–171. http://dx.doi.org/10.1016/j.marchem.2015.03.011.

Haley, B.A., Klinkhammer, G.P., Mix, A.C., 2005. Revisiting the rare earth elements in foraminiferal tests. Earth Planet. Sci. Lett. 239:79–97. http://dx.doi.org/10.1016/j.epsl.2005.08.014.

Helman, Y., Natale, F., Sherrell, R.M., LaVigne, M., Starovoytov, V., Gorbunov, M.Y., Falkowski, P.G., 2008. Extracellular matrix production and calcium carbonate precipitation by coral cells in vitro. Proc. Natl. Acad. Sci. U. S. A. 105:54–58. http://dx.doi.org/10.1073/pnas.0710604105.

Henry, L.V., Torres, J.J., 2013. Metabolism of an Antarctic solitary coral, *Flabellum impensum*. J. Exp. Mar. Biol. Ecol. 449:17–21. http://dx.doi.org/10.1016/j.jembe.2013.08.010.

Hines, S.K., Southon, J.R., Adkins, J.F., 2015. A high resolution record of Southern Ocean intermediate water radiocarbon over the past 30,000 years. Earth Planet. Sci. Lett. 432:46–58. http://dx.doi.org/10.1016/j.epsl.2015.09.038.

Hoy, S.K., Robinson, L.F., Scanlon, K.M., Waller, R.G., 2015. Processed EM-120 Multibeam Swath Bathymetry Collected During Nathaniel B. Palmer Cruises NBP08-05 and NBP11-03 (Grids and Associated Navigation). School of Earth Sciences, University of Bristol. 10.1594/PANGAEA.848195.

Igarashi, K., Akagi, T., Fu, F.-F., Yabuki, S., 2003. Determination of rare-earth elements in a limestone geological standard reference material by ICP-MS following solvent extraction. Anal. Sci. 19:441–445. http://dx.doi.org/10.2116/analsci.19.441.

Imai, N., Terashima, S., Itoh, S., Ando, A., 1996. 1996 compilation of analytical data on nine GSJ geochemical reference samples, "Sedimentary Rock Series". Geostand. Newslett. 20:165–216. http://dx.doi.org/10.1111/j.1751-908X.1996.tb00184.x.

IUPAC, 2014. Compendium of Chemical Terminology. second ed. Blackwell Scientific Publications, Oxford (the "Gold Book"), compiled by A. D. McNaught and A. Wilkinson. ((1997). XML on-line corrected version 2.3.3 (2014-02-24): http://goldbook.iupac.org (2006–) created by M. Nic, J. Jirat, B. Kosata; updates compiled by A. Jenkins, ISBN 0-9678550-9-8). 10.1351/goldbook.

Jackett, D.R., McDougall, T.J.M., 1997. A neutral density variable for the world's oceans. J. Phys. Oceanogr. 27:237–263. http://dx.doi.org/10.1175/1520-0485(1997)027<0237:ANDVFT>2.0.CO;2.

Jacobsen, S.B., Wasserburg, G.J., 1980. Sm-Nd isotopic evolution of chondrites. Earth Planet. Sci. Lett. 50:139–155. http://dx.doi.org/10.1016/0012-821X(80)90125-9.

Jeandel, C., 1993. Concentration and isotopic composition of Nd in the South Atlantic Ocean. Earth Planet. Sci. Lett. 117:581–591. http://dx.doi.org/10.1016/0012-821X(93)90104-H.

Kon, Y., Hoshino, M., Sanematsu, K., Morita, S., Tsunematsu, M., Okamoto, N., Yano, N., Tanaka, M., Takagi, T., 2014. Geochemical characteristics of apatite in heavy REE-rich deep-sea mud from Minamitorishima area, southeastern Japan. Resour. Geol. 64:47–57. http://dx.doi.org/10.2343/geochemj.2.0361.

Koeppenkastrop, D., De Carlo, E.H., 1992. Sorption of rare-earth elements from seawater onto synthetic mineral particles: an experimental approach. Chem. Geol. 95:251–263. http://dx.doi.org/10.1016/0009-2541(92)90015-W.

Lacan, F., Jeandel, C., 2004a. Subpolar mode water formation traced by neodymium isotopic composition. Geophys. Res. Lett. 31, L14306. http://dx.doi.org/10.1029/2004GL019747.

Lacan, F., Jeandel, C., 2004b. Neodymium isotopic composition and rare earth element concentrations in the deep and intermediate Nordic seas: constraints on the Iceland Scotland overflow water signature. Geochem. Geophys. Geosyst. 5, Q11006. http://dx.doi.org/10.1029/2004GC000742.

Lacan, F., Jeandel, C., 2005a. Acquisition of the neodymium isotopic composition of the North Atlantic deep water. Geochem. Geophys. Geosyst. 6, Q12008. http://dx.doi.org/10.1029/2005GC000956.

Lacan, F., Jeandel, C., 2005b. Neodymium isotopes as a new tool for quantifying exchange fluxes at the continent–ocean interface. Earth Planet. Sci. Lett. 232:245–257. http://dx.doi.org/10.1016/j.epsl.2005.01.004.

Lambelet, M.L., van de Flierdt, T., Crocket, K., Rehkämper, M., Kreissig, K., Coles, B., Rijkenberg, M.J.A., Gerringa, L.J.A., de Baar, H.J.W., Steinfeldt, R., 2016. Neodymium isotopic composition and concentration in the western North Atlantic Ocean: results from the GEOTRACES GA02 section. Geochim. Cosmochim. Acta 177:1–29. http://dx.doi.org/10.1016/j.gca.2015.12.019.

LaVigne, M., Matthews, K.A., Grottoli, A.G., Cobb, K.M., Anagnostou, E., Cabioch, G., Sherrell, R.M., 2010. Coral skeleton P/Ca proxy for seawater phosphate: multi-colony calibration with a contemporaneous seawater phosphate record. Geochim. Cosmochim. Acta 74:1282–1293. http://dx.doi.org/10.1016/j.gca.2009.11.002.

Lee, J.H., Byrne, R.H., 1993. Complexation of trivalent rare earth elements (Ce, Eu, Gd, Tb, Yb) by carbonate ions. Geochim. Cosmochim. Acta 57:295–302. http://dx.doi.org/10.1016/0016-7037(93)90432-V.

Lee, J.-M.S., Eltgroth, F., Boyle, E.A., Adkins, J.F., 2017. The transfer of bomb radiocarbon and anthropogenic lead to the deep North Atlantic Ocean observed from a deep sea coral. Earth Planet. Sci. Lett. 458:223–232. http://dx.doi.org/10.1016/j.epsl.2016.10.049.

Locarnini, R.A., Mishonov, A.V., Antonov, J.I., Boyer, T.P., Garcia, H.E., Baranova, O.K., Zweng, M.M., Paver, C.R., Reagan, J.R., Johnson, D.R., Hamilton, M., Seidov, D., 2013. World Ocean Atlas 2013. In: Levitus, S. (Ed.)In: Mishonov, A. (Ed.)Volume 1: Temperature 73. NOAA Atlas NESDIS Technical Ed. (40 pp).

López Correa, M., Montagna, P., Joseph, N., Rüggeberg, A., Fietzke, J., Flögel, S., Dorschel, B., Goldstein, S.L., Wheeler, A., Freiwald, A., 2012. Preboreal onset of cold-water coral growth beyond the Arctic Circle revealed by coupled radiocarbon and U-series dating and neodymium isotopes. Quat. Sci. Rev. 34:24–43. http://dx.doi.org/10.1016/j.quascirev.2011.12.005.

Margolin, A.R., Robinson, L.F., Burke, A., Waller, R.G., Scanlon, K.M., Roberts, M.L., Auro, M.E., van de Flierdt, T., 2014. Temporal and spatial distributions of cold-water corals in the Drake Passage: insights from the last 35,000 years. Deep-Sea Res. Pt. II 99:237–248. http://dx.doi.org/10.1016/j.dsr2.2013.06.008.

Martin, E.E., Blair, S.W., Kamenov, G.D., Scher, H.D., Bourbon, E., Basak, C., Newkirk, D.N., 2010. Extraction of Nd isotopes from bulk deep sea sediments for paleoceanographic studies on Cenozoic time scales. Chem. Geol. 269:414–431. http://dx.doi.org/10.1016/j.chemgeo.2009.10.016.

Martínez-Botí, M.A., Vance, D., Mortyn, P.G., 2009. Nd/Ca ratios in plankton-towed and core top foraminifera: confirmation of the water column acquisition of nd. Geochem. Geophys. Geosyst. 10, Q08018. http://dx.doi.org/10.1029/2009GC002701.

Mason, H.E., Montagna, P., Kubista, L., Taviani, M., McCulloch, M., Phillips, B.L., 2011. Phosphate defects and apatite inclusions in coral skeletal aragonite revealed by solid-state NMR spectroscopy. Geochim. Cosmochim. Acta 75:7446–7457. http://dx.doi.org/10.1016/j.gca.2011.10.002.

Montagna, P., McCulloch, M., Taviani, M., Remia, A., Rouse, G., 2005. High-resolution trace and minor element compositions in deep-water scleractinian corals (*Desmophyllum dianthus*) from the Mediterranean Sea and the Great Australian Bight. In: Freiwald, A., Roberts, J.M. (Eds.), Cold-Water Corals and Ecosystems. Springer, Berlin Heidelberg, Berlin, Heidelberg:pp. 1109–1126 (Available at:) http://dx.doi.org/10.1007/3-540-27673-4_56.

Montagna, P., McCulloch, M., Taviani, M., Mazzoli, C., Vendrell, B., 2006. Phosphorus in cold-water corals as a proxy for seawater nutrient chemistry. Science 312:1788–1791. http://dx.doi.org/10.1126/science.1125781.

Montagna, P., McCulloch, M., Douville, E., López Correa, M., Trotter, J., Rodolfo-Metalpa, R., Dissard, D., Ferrier-Pagès, C., Frank, N., Freiwald, A., Goldstein, S., Mazzoli, C., Reynaud, S., Rüggeberg, A., Russo, S., Taviani, M., 2014. Li/Mg systematics in scleractinian corals: calibration of the thermometer. Geochim. Cosmochim. Acta 132:288–310. http://dx.doi.org/10.1016/j.gca.2014.02.005.

Montero-Serrano, J.-C., Frank, N., Colin, C., Wienberg, C., Eisele, M., 2011. The climate influence on the mid-depth northeast Atlantic gyres viewed by cold-water corals. Geophys. Res. Lett. 38, L19604. http://dx.doi.org/10.1029/2011GL048733.

Montero-Serrano, J.-C., Frank, N., Tisnérat-Laborde, N., Colin, C., Wu, C.-C., Lin, K., Shen, C.-C., Copard, K., Orejas, C., Gori, A., De Mol, L., Van Rooij, D., Reverdin, G., Douville, E., 2013. Decadal changes in the mid-depth water mass dynamic of the northeastern Atlantic margin (Bay of Biscay). Earth Planet. Sci. Lett. 364:134–144. http://dx.doi.org/10.1016/j.epsl.2013.01.012.

Noble, T.L., Piotrowski, A.M., Robinson, L.F., McManus, J.F., Hillenbrand, C.-D., Bory, A.J.-M., 2012. Greater supply of Patagonian-sourced detritus and transport by the ACC to the Atlantic sector of the Southern Ocean during the last glacial period. Earth Planet. Sci. Lett. 317–318:374–385. http://dx.doi.org/10.1016/j.epsl.2011.10.007.

Orejas, C., Gori, A., Gili, J.M., 2008. Growth rates of live *Lophelia pertusa* and *Madrepora oculata* from the Mediterranean Sea maintained in aquaria. Coral Reefs 27:255. http://dx.doi.org/10.1007/s00338-007-0350-7.

Orsi, A.H., Whitworth III, T., Nowlin Jr., W.D., 1995. On the meridional extent and fronts of the Antarctic circumpolar current. Deep-Sea Res. Pt. I 42:641–673. http://dx.doi.org/10.1016/0967-0637(95)00021-W.

Orsi, A.H., Johnson, G.C., Bullister, J.L., 1999. Circulation, mixing, and production of Antarctic bottom water. Prog. Oceanogr. 43:55–109. http://dx.doi.org/10.1016/S0079-6611(99)00004-X.

Palmer, M.R., 1985. Rare earth elements in foraminifera tests. Earth Planet. Sci. Lett. 73:285–298. http://dx.doi.org/10.1016/0012-821X(85)90077-9.

Pearce, C.R., Jones, M.T., Oelkers, E.H., Pradoux, C., Jeandel, C., 2013. The effect of particulatedissolution on the neodymium (Nd) isotope and Rare Earth Element (REE) composition of seawater. Earth Planet. Sci. Lett. 369–370:138–147. http://dx.doi.org/10.1016/j.epsl.2013.03.023.

Piepgras, D.J., Wasserburg, G.J., 1982. Isotopic composition of neodymium in waters from the Drake Passage. Science 217:207–214. http://dx.doi.org/10.1126/science.217.4556.207.

Pin, C., Zalduegui, J.S., 1997. Sequential separation of light rare-earth elements, thorium and uranium by miniaturized extraction chromatography: application to isotopic analyses of silicate rocks. Anal. Chim. Acta 339:79–89. http://dx.doi.org/10.1016/S0003-2670(96)00499-0.

Przeniosło, R., Stolarski, J., Mazur, M., Brunelli, M., 2008. Hierarchically structured scleractinian coral biocrystals. J. Struct. Biol. 161:74–82. http://dx.doi.org/10.1016/j.jsb.2007.09.020.

Raddatz, J., Rüggeberg, A., Flögel, S., Hathorne, E.C., Liebetrau, V., Eisenhauer, A., Dullo, W.-C., 2014. The influence of seawater pH on U/Ca ratios in the scleractinian cold-water coral *Lophelia pertusa*. Biogeosciences 11, 1863–1871.

Reimer, P.J., Baillie, M.G.L., Bard, E., Bayliss, A., Beck, J.W., Blackwell, P.G., Ramsey, C.B., Buck, C.E., Burr, G.S., Edwards, R.L., Friedrich, M., Grootes, P.M., Guilderson, T.P., Hajdas, I., Heaton, T.J., Hogg, A.G., Hughen, K.A., Kaiser, K.F., Kromer, B., McCormac, F.G., Manning, S.W., Reimer, R.W., Richards, D.A., Southon, J.R., Talamo, S., Turney, C.S.M., van der Plicht, J., Weyhenmeyer, C.E., 2009. IntCal09 and Marine09 radiocarbon age calibration curves, 0–50,000 years cal BP. Radiocarbon 51:1111–1150 (Available at: https://journals.uair.arizona.edu/index.php/radiocarbon/article/view/3569).

Reynard, B., Lécuyer, C., Grandjean, P., 1999. Crystal-chemical controls on rare-earth element concentrations in fossil biogenic apatites and implications for paleoenvironmental reconstructions. Chem. Geol. 155:233–241. http://dx.doi.org/10.1016/S0009-2541(98)00169-7.

Rickli, J., Gutjahr, M., Vance, D., Fischer-Gödde, M., Hillenbrand, C.-D., Kuhn, G., 2014. Neodymium and hafnium boundary contributions to seawater along the West Antarctic continental margin. Earth Planet. Sci. Lett. 394:99–110. http://dx.doi.org/10.1016/j.epsl.2014.03.008.

Risk, M.J., Heikoop, J.M., Snow, M.G., Beukens, R., 2002. Lifespans and growth patterns of two deep-sea corals: *Primnoa resedaeformis* and *Desmophyllum cristagalli*. Hydrobiologia 471:125–131. http://dx.doi.org/10.1023/A:1016557405185.

Roberts, N.L., Piotrowski, A.M., Elderfield, H., Eglinton, T.I., Lomas, M.W., 2012. Rare earth element association with foraminifera. Geochim. Cosmochim. Acta 94:57–71. http://dx.doi.org/10.1016/j.gca.2012.07.009.

Robinson, L.F., Belshaw, N.S., Henderson, G.M., 2004. U and Th concentrations and isotope ratios in modern carbonates and waters from the Bahamas. Geochim. Cosmochim. Acta 68:1777–1789. http://dx.doi.org/10.1016/j.gca.2003.10.005.

Robinson, L.F., Adkins, J.F., Fernandez, D.P., Burnett, D.S., Wang, S.-L., Gagnon, A.C., Krakauer, N., 2006. Primary U distribution in scleractinian corals and its implications for U series dating. Geochem. Geophys. Geosyst. 7, Q05022. http://dx.doi.org/10.1029/2005GC001138.

Robinson, L.F., Noble, T.L., McManus, J.F., 2008. Measurement of adsorbed and total 232Th/230Th ratios from marine sediments. Chem. Geol. 252:169–179. http://dx.doi.org/10.1016/j.chemgeo.2008.02.015.

Robinson, L.F., van de Flierdt, T., 2009. Southern Ocean evidence for reduced export of North Atlantic Deep Water during Heinrich event 1. Geology 37:195–198. http://dx.doi.org/10.1130/G25363A.1.

Robinson, L.F., Adkins, J.F., Scheirer, D.S., Fernandez, D.P., Gagnon, A., Waller, R.G., 2007. Deep-sea scleractinian coral age and depth distributions in the northwest Atlantic for the last 225,000 years. Bull. Mar. Sci. 81, 371–391.

Robinson, L.F., Adkins, J.F., Frank, N., Gagnon, A.C., Prouty, N.G., Brendan Roark, E., van de Flierdt, T., 2014. The geochemistry of deep-sea coral skeletons: a review of vital effects and applications for palaeoceanography. Deep-Sea Res. Pt. II 99:184–198. http://dx.doi.org/10.1016/j.dsr2.2013.06.005.

Rollion-Bard, C., Blamart, D., 2015. Possible controls on Li, Na, and Mg incorporation into aragonite coral skeletons. Chem. Geol. 396:98–111. http://dx.doi.org/10.1016/j.chemgeo.2014.12.011.

Ryan, W.B.F., Carbotte, S.M., Coplan, J.O., O'Hara, S., Melkonian, A., Arko, R., Weissel, R.A., Ferrini, V., Goodwillie, A., Nitsche, F., Bonczkowski, J., Zemsky, R., 2009. Global multi-resolution topography synthesis. Geochem. Geophys. Geosyst. 10, Q03014. http://dx.doi.org/10.1029/2008GC002332.

Sabatier, P., Reyss, J.-L., Hall-Spencer, J.M., Colin, C., Frank, N., Tisnérat-Laborde, N., Bordier, L., Douville, E., 2012. ^{210}Pb-^{226}Ra chronology reveals rapid growth rate of *Madrepora oculata* and *Lophelia pertusa* on world's largest cold-water coral reef. Biogeosciences 9:1253–1265. http://dx.doi.org/10.5194/bg-9-1253-2012.

Schlitzer, R., 2012. Ocean Data View. http://odv.awi.de.

Shaw, H., Wasserburg, G., 1985. Sm-Nd in marine carbonates and phosphates: Implications for Nd isotopes in seawater and crustal ages. Geochim. Cosmochim. Acta 49:503–518. http://dx.doi.org/10.1016/0016-7037(85)90042-0.

Sholkovitz, E.R., Landing, W.M., Lewis, B.L., 1994. Ocean particle chemistry: the fractionation of rare earth elements between suspended particles and seawater. Geochim. Cosmochim. Acta 58:1567–1579. http://dx.doi.org/10.1016/0016-7037(94)90559-2.

Sholkovitz, E., Shen, G.T., 1995. The incorporation of rare earth elements in modern coral. Geochim. Cosmochim. Acta 59:2749–2756. http://dx.doi.org/10.1016/0016-7037(95)00170-5.

Sievers, H.A., Nowlin, W.D., 1984. The stratification and water masses at Drake Passage. J. Geophys. Res. 89:10489–10514. http://dx.doi.org/10.1029/JC089iC06p10489.

Sinclair, D.J., Williams, B., Risk, M., 2006. A biological origin for climate signals in corals—Trace element "vital effects" are ubiquitous in Scleractinian coral skeletons. Geophys. Res. Lett. 33:L17707. http://dx.doi.org/10.1029/2006GL027183.

Spooner, P.T., Chen, T., Robinson, L.F., Coath, C.D., 2016. Rapid uranium-series age screening of carbonates by laser ablation mass spectrometry. Quat. Geochronol. 31:28–39. http://dx.doi.org/10.1016/j.quageo.2015.10.004.

Squires, D.F., 1961. Deep sea corals collected by the Lamont Geological Observatory, 2, Scotia Sea corals. Amer. Mus. Novit. 2046:1–48 (URI: http://hdl.handle.net/2246/3482).

Stanley Jr., J.K., Byrne, R.H., 1990. The influence of solution chemistry on REE uptake by *Ulva lactuca* L. in seawater. Geochim. Cosmochim. Acta 54, 1587–1595.

Stichel, T., Frank, M., Rickli, J., Haley, B.A., 2012. The hafnium and neodymium isotope composition of seawater in the Atlantic sector of the southern ocean. Earth Planet. Sci. Lett. 317–318:282–294. http://dx.doi.org/10.1016/j.epsl.2011.11.025.

Stolarski, J., 2003. Three-dimensional micro- and nanostructural characteristics of the scleractinian coral skeleton: a biocalcification proxy. Acta Palaeontol. Pol. 48, 497–530.

Struve, T., 2016. Deciphering Glacial-interglacial Southern Ocean Dynamics With Deep-sea Corals. (PhD Thesis). Imperial College London.

Struve, T., van de Flierdt, T., Robinson, L.F., Bradtmiller, L.I., Hines, S.K., Adkins, J.F., Lambelet, M., Crocket, K.C., Kreissig, K., Coles, B., Auro, M.E., 2016. Neodymium isotope analyses after combined extraction of actinide and lanthanide elements from seawater and deep-sea coral aragonite. Geochem. Geophys. Geosyst. 17:232–240. http://dx.doi.org/10.1002/2015GC006130.

Sudre, J., Garçon, V., Provost, C., Sennéchael, N., Huhn, O., Lacombe, M., 2011. Short-term variations of deep water masses in Drake Passage revealed by a multiparametric analysis of the ANT-XXIII/3 bottle data. Deep-Sea Res. Pt. II 58:2592–2612. http://dx.doi.org/10.1016/j.dsr2.2011.01.005.

Talley, L.D., McCartney, M.S., 1982. Distribution and circulation of Labrador sea water. J. Phys. Oceanogr. 12:1189–1205. http://dx.doi.org/10.1175/1520-0485(1982)012<1189:DACOLS>2.0.CO;2.

Tanaka, T., Togashi, S., Kamioka, H., Amakawa, H., Kagami, H., Hamamoto, T., Yuhara, M., Orihashi, Y., Yoneda, S., Shimizu, H., Kunimaru, T., Takahashi, K., Yanagi, T., Nakano, T., Fujimaki, H., Shinjo, R., Asahara, Y., Tanimizu, M., Dragusanu, C., 2000. JNdi-1: a neodymium isotopic reference in consistency with LaJolla neodymium. Chem. Geol. 168:279–281. http://dx.doi.org/10.1016/S0009-2541(00)00198-4.

Taylor, S.R., McLennan, S.M., 1985. The Continental Crust: Its Composition and Evolution. Blackwell Scientific Pub, Palo Alto, CA.

Terakado, Y., Masuda, A., 1988. The coprecipitation of rare-earth elements with calcite and aragonite. Chem. Geol. 69:103–110. http://dx.doi.org/10.1016/0009-2541(88)90162-3.

Thiagarajan, N., Gerlach, D., Roberts, M.L., Burke, A., McNichol, A., Jenkins, W.J., Subhas, A.V., Thresher, R.E., Adkins, J.F., 2013. Movement of deep-sea coral populations on climatic timescales. Paleoceanography 28:227–236. http://dx.doi.org/10.1002/palo.20023.

Vance, D., Scrivner, A.E., Beney, P., Staubwasser, M., Henderson, G.M., Slowey, N.C., 2004. The use of foraminifera as a record of the past neodymium isotope composition of seawater. Paleoceanography 19, PA2009. http://dx.doi.org/10.1029/2003PA000957.

van de Flierdt, T., Robinson, L.F., Adkins, J.F., Hemming, S.R., Goldstein, S.L., 2006a. Temporal stability of the neodymium isotope signature of the Holocene to glacial North Atlantic. Paleoceanography 21, PA4102. http://dx.doi.org/10.1029/2006PA001294.

van de Flierdt, T., Hemming, S.R., Goldstein, S.L., Abouchami, W., 2006b. Radiogenic isotope fingerprint of Wilkes land–Adélie coast bottom water in the circum-Antarctic Ocean. Geophys. Res. Lett. 33, L12606. http://dx.doi.org/10.1029/2006GL026020.

van de Flierdt, T., Frank, M., 2010. Neodymium isotopes in paleoceanography. Quat. Sci. Rev. 29:2439–2441. http://dx.doi.org/10.1016/j.quascirev.2010.07.001.

van de Flierdt, T., Robinson, L.F., Adkins, J.F., 2010. Deep-sea coral aragonite as a recorder for the neodymium isotopic composition of seawater. Geochim. Cosmochim. Acta 74:6014–6032. http://dx.doi.org/10.1016/j.gca.2010.08.001.

Webb, G.E., Nothdurft, L.D., Kamber, B.S., Kloprogge, J.T., Zhao, J.-X., 2009. Rare earth element geochemistry of scleractinian coral skeleton during meteoric diagenesis: a sequence through neomorphism of aragonite to calcite. Sedimentology 56:1433–1463. http://dx.doi.org/10.1111/j.1365-3091.2008.01041.x.

Weis, D., Kieffer, B., Maerschalk, C., Barling, J., de Jong, J., Williams, G.A., Hanano, D., Pretorius, W., Mattielli, N., Scoates, J.S., Goolaerts, A., Friedman, R.M., Mahoney, J.B., 2006. High-precision isotopic characterization of USGS reference materials by TIMS and MC-ICP-MS. Geochem. Geophys. Geosyst. 7, Q08006. http://dx.doi.org/10.1029/2006GC001283.

Well, R., Roether, W., Stevens, D.P., 2003. An additional deep-water mass in Drake Passage as revealed by 3He data. Deep-Sea Res. Pt. I 50:1079–1098. http://dx.doi.org/10.1016/S0967-0637(03)00050-5.

Wilson, S.A., 1997. The collection, preparation and testing of USGS reference material BCR-2, Columbia River, Basalt. U.S. Geological Survey Open-file Report (98-00x).

Wilson, D.J., Crocket, K.C., van de Flierdt, T., Robinson, L.F., Adkins, J.F., 2014. Dynamic intermediate ocean circulation in the North Atlantic during Heinrich Stadial 1: a radiocarbon and neodymium isotope perspective. Paleoceanography 29, 2014PA002674. http://dx.doi.org/10.1002/2014PA002674.

Wyndham, T., McCulloch, M., Fallon, S., Alibert, C., 2004. High-resolution coral records of rare earth elements in coastal seawater: biogeochemical cycling and a new environmental proxy3. Geochim. Cosmochim. Acta 68:2067–2080. http://dx.doi.org/10.1016/j.gca.2003.11.004.

Yashayaev, I., Bersch, M., van Aken, H.M., 2007. Spreading of the Labrador Sea water to the Irminger and Iceland basins. Geophys. Res. Lett. 34, L10602. http://dx.doi.org/10.1029/2006GL028999.